

1 **A synthesis of cloud condensation nuclei counter (CCNC)**
2 **measurements within the EUCAARI network**

3
4 **M. Paramonov¹, V.-M. Kerminen¹, M. Gysel², P. P. Aalto¹, M. O. Andreae³, E.**
5 **Asmi¹⁶, U. Baltensperger², A. Bougiatioti⁹, D. Brus^{16,17}, G. Frank⁵, N. Good^{6,*}, S.**
6 **S. Gunthe^{3,**}, L. Hao⁷, M. Irwin^{6,***}, A. Jaatinen⁷, Z. Jurányi^{2,****}, S. M. King^{8,*****}, A.**
7 **Kortelainen⁷, A. Kristensson⁵, H. Lihavainen¹⁶, M. Kulmala¹, U. Lohmann¹³, S. T.**
8 **Martin⁸, G. McFiggans⁶, N. Mihalopoulos⁹, A. Nenes^{4,14,15}, C. D. O'Dowd¹⁰, J.**
9 **Ovadnevaite¹⁰, T. Petäjä¹, U. Pöschl³, G. C. Roberts^{11,18}, D. Rose^{3,*****}, B.**
10 **Svenningsson⁵, E. Swietlicki⁵, E. Weingartner^{2,****}, J. Whitehead⁶, A.**
11 **Wiedensohler¹², C. Wittbom⁵ and B. Sierau¹³**

12 [1] {Department of Physics, University of Helsinki, P.O. Box 64, FI-00014, Helsinki, Finland}

13 [2] {Laboratory of Atmospheric Chemistry, Paul Scherrer Institute, 5232 Villigen PSI,
14 Switzerland}

15 [3] {Biogeochemistry and Multiphase Chemistry Departments, Max Planck Institute for
16 Chemistry, Mainz, Germany}

17 [4] {School of Earth and Atmospheric Sciences, Georgia Institute of Technology, Atlanta GA
18 30332, USA}

19 [5] {Division of Nuclear Physics, Department of Physics, Lund University, P.O. Box 118, SE-
20 22100 Lund, Sweden}

21 [6] {Centre for Atmospheric Science, SEAES, The University of Manchester, Oxford Road,
22 Manchester M13 9PL, UK}

23 [7] {Department of Applied Physics, University of Eastern Finland, FI-70210, Kuopio,
24 Finland}

25 [8] {School of Engineering and Applied Sciences & Department of Earth and Planetary
26 Sciences, Harvard University, Cambridge MA 02138, USA}

27 [9] {Environmental Chemical Processes Laboratory, University of Crete, Heraklion, Greece}

1 [10] {School of Physics and Centre for Climate and Air Pollution Studies, Ryan Institute,
2 National University of Ireland Galway, University Road, Galway, Ireland}

3 [11] {Centre National de Recherches Météorologiques, Toulouse, France}

4 [12] {Leibniz Institute for Tropospheric Research, Leipzig, Germany}

5 [13] {Institute for Atmospheric and Climate Science, ETH Zurich, Zurich, Switzerland}

6 [14] {School of Chemical and Biomolecular Engineering, Georgia Institute of Technology,
7 Atlanta GA 30332, USA}

8 [15] {Institute of Chemical Engineering Sciences (ICE-HT), FORTH, Patras, Greece}

9 [16] {Finnish Meteorological Institute, Erik Palménin aukio 1, P.O. Box 503, FI-00101
10 Helsinki, Finland}

11 [17] {Laboratory of Aerosols Chemistry and Physics, Institute of Chemical Process
12 Fundamentals, Academy of Sciences of the Czech Republic, Rozvojová 135, 165 02 Prague 6,
13 Czech Republic}

14 [18] {Scripps Institution of Oceanography, University of California San Diego, La Jolla CA
15 92093, USA}

16 *now at: Department of Mechanical Engineering, Colorado State University, Fort Collins,
17 Colorado, USA

18 **now at: Department of Civil Engineering, Indian Institute of Technology Madras, Chennai,
19 India

20 ***now at: Cambustion Ltd., Cambridge, UK

21 ****now at: Institute of Aerosol and Sensor Technology, University of Applied Sciences
22 Northwestern Switzerland, Windisch, Switzerland

23 *****now at: Haldor Topsøe A/S, Copenhagen, Denmark

24 *****now at: Institute for Atmospheric and Environmental Sciences, Goethe-University
25 Frankfurt am Main, Frankfurt am Main, Germany

26 Correspondence to: M. Paramonov (mikhail.paramonov@helsinki.fi), V.-M. Kerminen (veli-
27 matti.kerminen@helsinki.fi), M. Gysel (martin.gysel@psi.ch) and B. Sierau
28 (berko.sierau@env.ethz.ch)

1

2 **Abstract**

3 Cloud Condensation Nuclei Counter (CCNC) measurements performed at 14 locations around
4 the world within the EUCAARI framework have been analysed and discussed with respect to
5 the cloud condensation nuclei (CCN) activation and hygroscopic properties of the atmospheric
6 aerosol. The annual mean ratio of activated cloud condensation nuclei (N_{CCN}) to the total
7 number concentration of particles (N_{CN}), known as the activated fraction A , shows a similar
8 functional dependence on supersaturation S at many locations; exceptions to this being certain
9 marine locations, a free troposphere site and background sites in south-west Germany and
10 northern Finland. The use of total number concentration of particles above 50 and 100 nm
11 diameter when calculating the activated fractions (A_{50} and A_{100} , respectively) renders a much
12 more stable dependence of A on S ; A_{50} and A_{100} also reveal the effect of the size distribution on
13 CCN activation. With respect to chemical composition, it was found that the hygroscopicity of
14 aerosol particles as a function of size differs among locations. The hygroscopicity parameter κ
15 decreased with an increasing size at a continental site in south-west Germany and fluctuated
16 without any particular size dependence across the observed size range in the remote tropical
17 North Atlantic and rural central Hungary. At all other locations κ increased with size. In fact,
18 in Hyytiälä, Vavihill, Jungfraujoch and Pallas the difference in hygroscopicity between Aitken
19 and accumulation mode aerosol was statistically significant at the 5% significance level. In a
20 boreal environment the assumption of a size-independent κ can lead to a potentially substantial
21 overestimation of N_{CCN} at S levels above 0.6%; similar is true for other locations where κ was
22 found to increase with size. While detailed information about aerosol hygroscopicity can
23 significantly improve the prediction of N_{CCN} , total aerosol number concentration and aerosol
24 size distribution remain more important parameters. The seasonal and diurnal patterns of CCN
25 activation and hygroscopic properties vary among three long-term locations, highlighting the
26 spatial and temporal variability of potential aerosol-cloud interactions in various environments.

27

28 **1 Introduction**

29 Atmospheric aerosol particles are known to modify the microphysical properties of clouds, such
30 as their albedo, lifetime and precipitation patterns (Boucher et al., 2013). Due to the importance
31 of clouds in the weather and climate systems, these aerosol-induced changes, known as the
32 indirect effects of aerosols on climate, are a subject of rigorous research. The quantification of

1 the radiative forcing associated with the interactions of atmospheric aerosol with clouds
2 remains one of the biggest challenges in the current understanding of climate change (Boucher
3 et al., 2013). These challenges are associated with the production of the aerosol particles that
4 are able to activate into cloud droplets, known as cloud condensation nuclei (CCN) (e.g.
5 Laaksonen et al., 2005; Andreae and Rosenfeld, 2008; Kuang et al., 2009; Kerminen et al.,
6 2012), their actual activation into cloud drops (e.g. Kulmala et al., 1996; Dusek et al., 2006;
7 McFiggans et al., 2006; Paramonov et al., 2013; Hammer et al., 2014), the formation of clouds
8 (e.g. Twomey, 1959; Mason and Chien, 1962; Vaillancourt et al., 2002), time evolution of cloud
9 microphysical and other properties (e.g. Rosenfeld et al., 2014) and the interaction of clouds
10 with the solar and terrestrial radiation (e.g. Boucher and Lohmann, 1995; Ramanathan et al.,
11 2001; Chen et al., 2014). A better understanding is needed with respect to each of these steps
12 in order to improve the performance of the current global climate models (GCMs) and to
13 increase the accuracy of the future climate predictions.

14 Several aerosol properties are of special interest when looking at the interaction of atmospheric
15 aerosol particles with warm clouds. The current article focuses on the number, size and
16 hygroscopicity of the atmospheric aerosol particles with regard to how these parameters affect
17 the potential of particles to act as CCN. One such property of interest is the CCN number
18 concentration N_{CCN} . Depending on the location, N_{CCN} can vary by several orders of magnitude,
19 and it directly depends on the aerosol properties and the ambient water vapour supersaturation
20 ratio S in the atmosphere. Köhler theory dictates that the minimum size at which particles
21 activate into cloud drops decreases with increasing S (Köhler, 1936); consequently N_{CCN}
22 increases monotonically with S for a given aerosol population. The exact response of N_{CCN} to
23 an increasing S depends on the total aerosol number concentration N_{CN} , aerosol size distribution
24 and particle hygroscopicity. Besides the relevant references found throughout the paper,
25 discussion about N_{CCN} concentrations in various environments can be found in, e.g. Pandis et
26 al. (1994), Covert et al. (1998), Snider and Brenguier (2000), Chang et al. (2007), Andreae and
27 Rosenfeld (2008), Andreae (2009) and Wang et al. (2010). At any given S , another property of
28 interest is the critical dry diameter of CCN activation D_c , defined as the smallest diameter at
29 which particles activate into cloud drops. For internally mixed polydisperse aerosol particles,
30 this diameter indicates that in the presence of a sufficient amount of water vapour all particles
31 above this size activate into cloud drops, and all particles below this size do not. However,
32 atmospheric aerosol is frequently externally mixed, with particles of different sizes exhibiting
33 different chemical composition, and, therefore, in practice, D_c is usually estimated as the

1 diameter at which 50% of the particles activate and grow into cloud drops at any given S . D_c
2 can be directly calculated from size-segregated Cloud Condensation Nuclei Counter (CCNC)
3 measurements (Rose et al., 2008) or estimated from the size distribution data coupled with N_{CCN}
4 (Hitzenberger et al., 2003; Furutani et al., 2008). The effect of hygroscopicity on the activation
5 of CCN into cloud drops has also been studied extensively, and several simplified theoretical
6 models have been suggested to link particle composition with critical supersaturation S_c , i.e. the
7 minimum S required for the particles of a certain size to activate into cloud drops (e.g.
8 Svenningsson et al., 1992; Rissler et al., 2005; Khvorostyanov and Curry, 2007; Wex et al.,
9 2007). One such approach is the hygroscopicity parameter κ , also known as “kappa”, a unitless
10 number describing the cloud condensation nucleus activity (Petters and Kreidenweis, 2007).
11 The value of κ typically varies between zero and just above unity, with values close to zero
12 indicating a non-hygroscopic aerosol, i.e. with low affinity for water (e.g. freshly emitted black
13 carbon; e.g. Hudson et al., 1991; Weingartner et al., 1997; Wittbom et al., 2014) and values
14 close to unity indicating an aerosol with high hygroscopicity, i.e. high affinity for water (e.g.
15 sea salt particles; e.g. Good et al., 2010). Since its introduction, the parameter κ has been used
16 in CCN studies quite extensively (e.g. Carrico et al., 2008; Kammermann et al., 2010a; Levin
17 et al., 2014).

18 This article summarises the measurements performed by CCNCs within the framework of the
19 European Integrated project on Aerosol Cloud Climate and Air Quality interactions
20 (EUCAARI). One of the EUCAARI project aims was to compile a comprehensive database of
21 in situ measured aerosol, CCN and hygroscopic properties in order to increase the knowledge
22 about aerosol-cloud-climate interactions and to combine the relevant existing measurement
23 infrastructure (Kulmala et al., 2011). Besides CCNCs already deployed at the existing European
24 long-term measurement stations, several intensive field campaigns using the CCNC were
25 carried out as part of EUCAARI as well. The main objective of this work is to present a
26 comprehensive overview and intercomparison of CCNC measurements and to provide an
27 insight into the cloud droplet activation and aerosol hygroscopic properties in different
28 environments. More specifically, the aims are to i) get new insight into CCN number
29 concentrations and activated fractions around the world and their dependence on the water
30 vapour supersaturation ratio, ii) provide new information about the dependence of aerosol
31 hygroscopicity on particle size, and iii) reveal seasonal and diurnal variation of CCN activation
32 and hygroscopic properties. While undeniably important, the effect of size distribution on N_{CCN}
33 and the size-resolved activated fraction (e.g. Dusek et al., 2006; Quinn et al., 2008; Morales

1 Betancourt and Nenes, 2014) is not investigated herein, and an overview of the existing
2 EUCAARI aerosol size distribution data can be found in Asmi et al. (2011) and Beddows et al.
3 (2014).

4

5 **2 Methodology**

6 **2.1 Instrumentation**

7 A CCNC is a type of instrument frequently used for studying the cloud droplet activation
8 potential of aerosol particles. In its simplest setup, a CCNC consists of a saturator unit and an
9 optical particle counter (OPC) frequently running in parallel with a condensation particle
10 counter (CPC). For all measurements presented herein, the CCNC used was a commercially
11 available instrument produced by Droplet Measurement Technologies, Inc. (DMT-CCNC), the
12 basic principles of operation of which are described below.

13 Upon entering the measurement setup, the aerosol flow is split into two sample flows, with the
14 first flow leading to a CPC to determine the total particle number concentration, hereafter
15 referred to as N_{CN} . The second flow feeds the aerosol into the saturator unit of the CCNC, inside
16 of which the conditions of supersaturation S_{eff} with respect to water vapour down the centre of
17 the column are established. Aerosol, flowing under laminar flow conditions, is subjected to
18 these supersaturation conditions, during which particles with a critical supersaturation S_c
19 smaller than S_{eff} will grow by the condensation of water vapour and remain in stable
20 equilibrium, i.e. activate as CCN. The residence time inside the saturator column (~ 10 s) allows
21 for the activated particles to grow to sizes larger than $1\mu\text{m}$ in diameter; these particles are then
22 counted by the OPC providing the number concentration of activated aerosol particles, a
23 quantity hereafter referred to as N_{CCN} . The described setup is characteristic of polydisperse
24 measurements; an inclusion of a drier, a neutraliser and a Differential Mobility Analyzer (DMA;
25 Knutson and Whitby, 1975) prior to the splitting of the flow into two parallel lines allows for
26 the selection of a particular particle size, i.e. quasi-monodisperse measurements. Such
27 measurements can be performed either by varying the particle size at a constant S_{eff} (D -scan) or
28 by varying S_{eff} at a constant particle size (S -scan). Such a setup, while more complex, provides
29 activation spectra and allows for a direct calculation of the critical dry diameter of droplet
30 activation D_c (in case of the D -scan) or the critical supersaturation S_c (in case of the S -scan).
31 Typically, a CCNC operates at several different levels of S_{eff} , most commonly ranging between

1 0.1 and 1.0%; the deviations from the nominal assigned S_{eff} values can be monitored and
2 corrected by applying a standardized calibration procedure, as described in section 2.3. A more
3 detailed description of the general operating procedures of the CCNC can be found in Roberts
4 and Nenes (2005); exact details of the measurement setup at each of the locations described in
5 the next section can be found in the respective published literature referenced throughout the
6 text.

7 **2.2 Measurement sites**

8 Data from a total of 14 EUCAARI locations have been provided for this analysis, including
9 both long-term measurement stations and short-term campaigns (Figure 1). As seen in the
10 figure, datasets came from a wide variety of locations representing various environments,
11 including marine and continental, urban and background, at altitudes ranging from the ground
12 level to the free troposphere. The location and description of each measurement site is given in
13 Table 1. All measurements presented herein were performed within the EUCAARI framework.

14 Hyytiälä Forestry Field Station in Southern Finland is the location of the Station for Measuring
15 Ecosystem-Atmosphere Relations SMEAR II, operated by the University of Helsinki. Located
16 on a flat terrain and surrounded by the boreal coniferous forest, mainly Scots pine, the station
17 is well representative of the boreal environment (Hari and Kulmala, 2005). It is a rural
18 background site, with the nearest city of Tampere (pop. 220 000) located 50 km to the
19 southwest. Air masses at the site can be of both Arctic and European origin, however, aerosol
20 particle number concentrations at this site are typically low (Sogacheva et al., 2005).

21 Vavihill in Southern Sweden is a continental background site surrounded by grasslands and
22 deciduous forest and operated by Lund University. The site is located 60-70 km NNE of the
23 Malmö and Copenhagen urban area (pop. ~2 000 000), however, it is considered to not be
24 affected by the local anthropogenic sources (Tunved et al., 2003). Due to its location, the site
25 is often used for monitoring the transport of pollution from continental Europe into the Nordic
26 region (Tunved et al., 2003).

27 The Jungfraujoch is a high alpine station in the Bernese Alps in Switzerland, where the aerosol
28 measurements are performed by the Paul Scherrer Institute (PSI). Being located high in the
29 mountains (3580 m a.s.l.), the station is far from local sources of pollution and is, in fact, in the
30 free troposphere most of the time; hence, it is considered a continental background site and
31 aerosol concentrations are very low (Collaud Coen et al., 2011). However, particularly during

1 the summer months, the Jungfrauoch site is frequently influenced by the injections of more
2 polluted air from the planetary boundary layer, driven by thermal convection (Jurányi et al.,
3 2010; Kammermann et al., 2010a; Jurányi et al., 2011). The station is frequently inside clouds
4 allowing for direct measurements of aerosol-cloud interactions.

5 Mace Head is a coastal marine site located on the west coast of Ireland and operated by the
6 National University of Ireland, Galway. The distance to the nearest urban settlement of Galway
7 City (88 km, pop. 65 000) renders Mace Head a clean background site; being on the coast, the
8 station is directly exposed to the North Atlantic Ocean. Occasionally the station is subject to
9 more polluted air masses originating from continental Europe and the United Kingdom
10 (O'Dowd et al., 2014).

11 Pallas is a remote continental site in northern Finland located in the northernmost boreal forest
12 zone in Europe; it is run by the Finnish Meteorological Institute (FMI). The station is situated
13 on top of a treeless hill and, due to the frequent presence of clouds, is suitable for in situ
14 measurements of aerosol-cloud interactions. The Pallas station is subject to both clean Arctic
15 air masses, as well as to more polluted European air masses; regardless, absolute particle
16 number concentrations are typically low (Hatakka et al., 2003).

17 Finokalia station is a remote coastal site located on the island of Crete and operated by the
18 University of Crete. The station is located on top of a hill, and most frequently air masses arrive
19 in Finokalia over the Mediterranean Sea (Stock et al., 2011). The station is representative of
20 background conditions as there are no local sources of pollution present; the largest nearby
21 urban centre of Heraklion (pop. 175 000) is 50 km to the west.

22 The Cabauw Experimental Site for Atmospheric Research (CESAR) is located in the central
23 Netherlands, 44 km from the North Sea. The station is in a rural area, however, the big cities of
24 Utrecht and Rotterdam are nearby; the station is subject to both continental and maritime
25 conditions (Mensah et al., 2012). The station is operated by the Royal Netherlands
26 Meteorological Institute (KNMI).

27 The University of Manchester conducted four short-term measurement campaigns utilising a
28 CCNC: K-puszta, Chilbolton, COPS and RHaMBLe. K-puszta is a rural site surrounded by
29 deciduous/coniferous forest located on the Great Hungarian Plain in central Hungary 80 km SE
30 of Budapest. The site has no local anthropogenic pollution sources (Ion et al., 2005). Chilbolton
31 is also a rural site, located in southern United Kingdom, 100 km WSW of London. The site is
32 most frequently influenced by the marine air masses; a potential local source of anthropogenic

1 pollution is the seasonal agricultural spraying (Campanelli et al., 2012). The Convective and
2 Orographically-induced Precipitation Study (COPS) campaign took place at the top of the
3 Hornisgrinde Mountain in the Black Forest region of south-west Germany. While this site is
4 primarily surrounded by the coniferous forest, the close proximity to the Rhine Valley exposes
5 the site to some anthropogenic pollution. Due to its elevation, the site is occasionally in the free
6 troposphere (Jones et al., 2011). The Reactive Halogens in the Marine Boundary Layer
7 (RHAMBLE) Discovery Cruise D319 campaign was a cruise conducted in the tropical North
8 Atlantic between Portugal and Cape Verde. The operational area can be described as a remote
9 marine environment with few, if any, sources of anthropogenic pollution. Air masses can
10 originate from both the ocean and from the African mainland (Good et al., 2010).

11 The Max Planck Institute for Chemistry (MPIC) also conducted four CCNC measurement
12 campaigns within the EUCAARI framework: PRIDE-PRD2006, AMAZE-08, CAREBeijing-
13 2006 and CLACE-6, with the last one having taken place at the previously described
14 Jungfraujoch station. The PRIDE-PRD2006 campaign took place in southeastern China, in a
15 small village ~60 km NW of Guangzhou, in the vicinity of a densely populated urban centre.
16 The wind direction during the campaign rendered the site a rural receptor of the regional
17 pollution originating from the Guangzhou urban cluster (Rose et al., 2010). The AMAZE-08
18 campaign took place at a remote site in an Amazonian rainforest, 60 km NNW of Manaus.
19 During the campaign, the site experienced air masses characteristic of clean tropical rainforest
20 conditions as well as air masses influenced by long-range transport of pollution (Gunthe et al.,
21 2009; Martin et al., 2010). The CAREBeijing-2006 campaign was conducted at a suburban site
22 in northern China, on the grounds of Huang Pu University in Yufa, ~50 km south of Beijing.
23 The site is subject to air masses originating both in the south and in the north; however, being
24 located on the outskirts of a large urban centre, particle concentrations are generally high
25 (Garland et al., 2009).

26 **2.3 Data**

27 The measurement period for each location and a brief summary of available CCNC data are
28 presented in Figure 2 and Table 2, respectively. Available data range from mid-2006 to the end
29 of 2012; the four long-term datasets all exceed one year in duration. As originally requested by
30 the authors from the EUCAARI partners, some of the data were submitted in the NASA-Ames
31 format with daily and monthly/campaign averages. Other datasets were submitted in the
32 original time resolution and have been compiled accordingly for this overview study.

1 For the quality assurance of the CCNC data, data providers were requested to recalculate all
 2 values to correspond to the standard temperature and pressure and to utilise a consistent
 3 procedure for the CCNC calibration. Calibrations were asked to be performed as outlined in
 4 Rose et al. (2008) using nebulised, dried, charge-equilibrated and size-selected ammonium
 5 sulphate or sodium chloride aerosol particles. To predict S_{eff} for instrument calibration, water
 6 activity was asked to be parameterised according to either the AIM-based model (Rose et al.,
 7 2008) or the ADDEM-model (Topping et al., 2005); both of these models can be considered as
 8 accurate sources of water activity data, and the discussion about their associated uncertainties
 9 can be found in the corresponding references. As none of the participating data providers noted
 10 a deviation from the calibration procedure, it is assumed that the data were treated accordingly.
 11 However, deviations from the described procedure and from the target S_{eff} levels may be
 12 possible and can potentially affect some of the conclusions presented in this paper.
 13 Uncertainties associated with deviations from the mentioned calibration procedure and
 14 parameterisation are discussed in great detail in Rose et al. (2008) and Topping et al. (2005).

15 For some of the polydisperse datasets, where available, Differential/Scanning Mobility Particle
 16 Sizer (DMPS/SMPS; Wang and Flagan, 1989; Wiedensohler et al., 2012) data were used in
 17 conjunction with the CCNC to derive the critical dry diameter D_c . The procedure was carried
 18 out by comparing N_{CCN} to the DMPS/SMPS-derived number size distributions; these were
 19 integrated from the largest size bin until the cumulative N_{CN} concentration was equal to N_{CCN} .
 20 D_c was then calculated by interpolating between the two adjacent size bins (Furutani et al.,
 21 2008). Following the calculation of D_c , the hygroscopicity parameter κ was determined using
 22 the effective hygroscopicity parameter (EH1) Köhler model (Eq. 1) assuming the surface
 23 tension of pure water (Petters and Kreidenweis, 2007; Rose et al., 2008). Due to the surface
 24 tension of actual cloud droplets being lower than that of pure water droplets (Facchini et al.,
 25 2000), this assumption, although commonly used, typically leads to an overestimation of the
 26 N_{CCN} (Kammermann et al., 2010b).

$$27 \quad S = \frac{D_{\text{wet}}^3 - D_s^3}{D_{\text{wet}}^3 - D_s^3 (1 - \kappa)} \exp\left(\frac{4\sigma_{\text{sol}} M_w}{RT \rho_w D_{\text{wet}}}\right). \quad (1)$$

28 In Equation 1 S is water vapour saturation ratio, D_{wet} is the droplet diameter, D_s is the dry
 29 particle diameter, which, as per Rose et al. (2008), can be substituted with D_c , κ is the
 30 hygroscopicity parameter, σ_{sol} is the surface tension of condensing solution (assumed to be pure
 31 water), M_w is the molar mass of water, R is the universal gas constant, T is the absolute
 32 temperature and ρ_w is the density of pure water.

1 For certain sites, total number concentrations of particles larger than 50 nm or 100 nm in
2 diameter (N_{50} or N_{100}) were calculated from the corresponding DMPS or SMPS data.

3 In order to compare the results from different stations, several interpolation/extrapolation
4 techniques were used. All N_{CCN} concentrations were averaged for each site for each S_{eff} level
5 and then recalculated to correspond to the target S_{eff} levels suggested by the Aerosols, Clouds
6 and Trace gases Research InfraStructure (ACTRIS) Network: 0.1, 0.2, 0.3, 0.5 and 1.0%.
7 Recalculation to the nearest target supersaturation was accomplished by a simple linear
8 interpolation/extrapolation of N_{CCN} as a function of S_{eff} using the two adjacent/nearest S_{eff}
9 points. For the Jungfraujoch data, D_c at S_{eff} of 0.12% and 0.95% was recalculated to the
10 corresponding D_c at the target S_{eff} of 0.1% and 1.0%, respectively, assuming a size-independent
11 κ .

12

13 **3 Results and Discussion**

14 **3.1 CCN concentrations**

15 Table 3 presents CCN number concentrations N_{CCN} at all 18 measurements locations and
16 campaigns for five S_{eff} levels mentioned in the previous section. First and foremost, since CCN
17 are simply a fraction of the total aerosol population with their concentration depending on S_{eff} ,
18 N_{CCN} values at S_{eff} of 1.0% follow a similar pattern known from total particle number
19 concentrations. The lowest N_{CCN} values, thus, originate in remote and clean locations, such as
20 Pallas, the Amazonian rainforest (AMAZE-08), Jungfraujoch and Chilbolton. The highest N_{CCN}
21 values are found in more polluted locations – CAREBeijing-2006 and PRIDE-PRD2006, both
22 in China. At lower S_{eff} levels, other effects, such as those of size distribution and hygroscopicity,
23 become more pronounced. When examining N_{CCN} at S_{eff} of 0.1%, the highest values are still
24 found in China; similar to N_{CCN} at S_{eff} of 1.0%, the lowest values are found in Pallas, the
25 Amazonian rainforest (AMAZE-08), Jungfraujoch and also in south-west Germany (COPS).

26 In order to examine the CCN activation spectra in more detail, Figure 3 presents cumulative
27 N_{CCN} concentrations shown as percentage of the N_{CCN} measured at the highest S_{eff} of 1.0%. One
28 group of locations that can be pointed out in the figure is representative of the marine
29 environment: Finokalia, Mace Head and the RHaMBLe campaign. At these marine locations
30 the presence of large and hygroscopic sea salt particles is expected, and a large fraction of
31 particles already activates at the lowest S_{eff} , i.e. of the total N_{CCN} measured at the highest S_{eff} ,

1 about a third activates already at the lowest S_{eff} . In the case of Mace Head, the observed
2 behaviour is due to the presence of sea salt particles and a peculiar organic composition of the
3 marine aerosol (Ovadnevaite et al., 2011). Additionally, both Finokalia and Mace Head have a
4 large fraction of the long-range transported and aged aerosol (Bougiatioti et al., 2009;
5 Ovadnevaite et al., 2011), which has been shown to increase particle hygroscopicity (Perry et
6 al., 2004; Furutani et al., 2008). Chilbolton, being a continental background site representative
7 of the regional aerosol properties, also belongs to this group; however, the N_{CCN} concentrations
8 at this location may be underestimated due to the aerosol not being dried prior to entering the
9 CCNC (Whitehead et al., 2014).

10 Another group of locations with a different CCN activation pattern is represented by Pallas and
11 Cabauw – at these locations very few particles activate at the lowest S_{eff} , and the N_{CCN} increases
12 drastically when S_{eff} changes from 0.5% to 1.0%. This may indicate that the aerosol is
13 dominated by the Aitken mode particles and, to a lesser extent, that the aerosol may be of low
14 hygroscopicity. A high concentration of Aitken mode particles in the autumn and low aerosol
15 hygroscopicity in Pallas have been previously reported by Tunved et al. (2003) and Komppula
16 et al. (2006), respectively. The two measurement locations discussed here are interesting with
17 regard to the ratio of presumed cloud droplet number concentration (CDNC) to the total aerosol
18 particle number concentration. It has been reported that, although under the clean and
19 convective conditions ambient S_c may reach as high as 1.0%, in the polluted boundary layer S_c
20 usually remains below 0.3% (Ditas et al., 2012; Hammer et al., 2014; Hudson and Noble, 2014).
21 If one assumes this value, a comparatively small fraction of aerosol in northern Finland and
22 central Netherlands would potentially activate into cloud droplets if exposed to this S_c . This has
23 direct implications for the cloud formation and, thus, local climate at these locations.

24 **3.2 Activated fraction**

25 Another variable describing CCN activation properties of an aerosol population that was
26 examined for the majority of locations is the activated fraction A calculated as a ratio of N_{CCN}
27 to N_{CN} (Figure 4). Each activation curve in Figure 4 is based on the arithmetic mean values of
28 A calculated from all available data for each station for each S_{eff} level. Included in the figure is
29 the overall fit shown with prediction bounds (95% confidence level) based on most of the
30 activation curves, except the outlying ones of Finokalia, COPS, Jungfraujoch and Pallas A, B
31 and C. As can be seen in the figure from the similar shape and placement of the activation
32 curves and in the Table 4 from the similar slope and intercept values, for many locations there

1 is no discernible difference in how A responds to changing S_{eff} on an annual basis; this is further
2 signified by the prediction bounds of the overall fit. Therefore, the average total number
3 concentration N_{CN} alone is sufficient in order to roughly estimate the annual mean N_{CCN} at any
4 given S_{eff} , for example, using the overall fit parameters presented in Table 4. The
5 appropriateness of the overall fit for estimating N_{CCN} based on N_{CN} alone was investigated for
6 the whole Hyytiälä dataset, by comparing the N_{CCN} measured by the CCNC with the N_{CCN}
7 calculated using the N_{CN} and the overall fit presented in Table 4. Such a comparison revealed
8 that for Hyytiälä the overall fit leads to an annual median overestimation of N_{CCN} of 49, 41, 33,
9 17 and 2% for the S_{eff} levels of 0.1, 0.2, 0.3, 0.5 and 1.0%, respectively.

10 For S_{eff} levels below 0.3% the variability of the overall fit, as shown by the prediction bounds,
11 leads to the uncertainty of the predicted N_{CCN} of up to an average of $\sim 45\%$. This uncertainty
12 decreases exponentially for S_{eff} levels above 0.3%. A global modelling study conducted by
13 Moore et al. (2013) reported that CDNC over the continental regions is fairly insensitive to
14 N_{CCN} , where a 4–71% uncertainty in N_{CCN} leads to a 1–23% uncertainty in CDNC. Since the
15 overwhelming majority of measurements analysed in this paper were conducted on land, and
16 the overall fit results in an uncertainty of the predicted annual mean N_{CCN} of up to $\sim 45\%$, for
17 many sites the use of the overall fit would yield a deviation of the predicted average CDNC of
18 approximately less than 10%. CDNC, however, is more sensitive to N_{CCN} in cleaner regions
19 with low total particle number concentrations, such as the Alaskan Arctic and remote oceans
20 (Moore et al., 2013). In such areas the use of the overall fit may not be appropriate.

21 Four locations stand out in Figure 4 which were not included in the overall fit. A is visibly
22 higher in Finokalia and during the COPS campaign than in other locations, with approximately
23 60% of the total aerosol population at both locations activating into cloud drops at the S_{eff} of
24 $\sim 0.4\%$. Reasons for the observed behaviour in Finokalia were discussed in the preceding section
25 3.1. During the COPS campaign the size distributions varied greatly, and, as will be shown
26 later, Aitken mode aerosol was more hygroscopic than accumulation mode aerosol, possibly
27 explaining the behaviour of the COPS activation curve seen in Figure 4 at least for higher S_{eff}
28 levels (Irwin et al., 2010; Jones et al., 2011). Another location with seemingly different
29 activation curves is Pallas, where the activation spectrum changes throughout the year, and even
30 at fairly high S_{eff} level of 1.0%, less than half of the total aerosol population activated into cloud
31 drops. The long-term Jungfraujoch dataset also exhibited comparatively low A values, lower
32 than those presented by Jurányi et al. (2011) and those during the CLACE-6 campaign at the

1 same location (Fig. 4). While the A values in the long-term Jungfraujoch dataset were calculated
2 with respect to CPC measurements of total particle number concentration, A values for the
3 CLACE-6 campaign and those reported by Jurányi et al. (2011) were calculated with respect to
4 integrated SMPS size distribution measurements with a higher size cutoff. While the aerosol
5 hygroscopicity at these locations will be discussed later, the effect of the size distribution on
6 the activation curves is evident.

7 The similarity in how A responds to S_{eff} at the majority of studied locations is an interesting
8 result. In other words, at any given S_{eff} the annual mean fraction of aerosol that will activate
9 into cloud drops is pretty much the same in many locations, a fact that was pointed out
10 previously by Andreae (2009). This phenomenon can easily be illustrated using the example of
11 the activation curve during the RHaMBLe cruise in the tropical North Atlantic. As will be
12 discussed later, while the N_{CCN} here is comparable to several other locations, the hygroscopicity
13 of the aerosol is much higher, with the hygroscopicity parameter κ being just below unity across
14 all studied sizes. Yet, the fact that the aerosol is so hygroscopic seems to affect the activation
15 efficiency of the aerosol in a similar manner as, for example, during the PRIDE-PRD2006
16 campaign in southeastern China. During this campaign absolute N_{CCN} was an order of
17 magnitude higher than during the RHaMBLe cruise (Table 2), and the hygroscopicity was much
18 lower (Rose et al., 2010). This order of magnitude difference in N_{CCN} , a large difference in κ
19 and at least some presumed difference in the shape of size distribution between the RHaMBLe
20 cruise and the PRIDE-PRD2006 campaign seem to result in no apparent difference in the
21 fraction of the aerosol that activates into cloud drops at any given S_{eff} . For most of the
22 continental locations the overall fit presented in Table 4 can provide a reasonable estimation of
23 annual mean N_{CCN} based on the N_{CN} for any given S_{eff} . It should be kept in mind, however, that
24 the activation curves in Fig. 4 for the long-term datasets do not reflect the potential short-term
25 or seasonal variability, which, as can be seen in the example of the three Pallas campaigns, can
26 be rather high. This and the fact that the short-term campaigns have been conducted during
27 different seasons mean that the overall fit represents the annual mean activation behaviour and
28 does not capture the variability on the shorter time scales.

29 One important uncertainty associated with the comparison of the activation curves in Figure 4
30 is the precise size range from which N_{CN} is determined. In order for the activation curves to be
31 directly comparable, the lower size limit of N_{CN} must be the same for all locations. In this study,
32 data of the lower limit of N_{CN} for each location ($N_{\text{CN,Dmin}}$) were unavailable and, hence, this

1 parameter was likely to vary, complicating the comparison of activation curves in Figure 4. To
2 circumvent the problem, to conduct a more accurate comparison and to reveal more information
3 about the effect of size distribution on CCN variability, N_{100} and N_{50} concentrations were used
4 instead of N_{CN} to calculate the effective activated fractions corresponding to a certain lower
5 cutoff diameter A_{100} and A_{50} , respectively. These were calculated for the four long-term
6 measurement locations only (where the data were available), and the results of the comparison
7 are depicted in Figure 5. When N_{100} is used instead of N_{CN} , the differences among locations
8 described above almost disappear except for the lowest values of S . In general, the activation
9 curve of A_{100} for Mace Head is similar to those for Hyytiälä, Vavihill and Jungfraujoch for S_{eff}
10 above 0.4%. In other words, when one considers the fraction of only accumulation mode
11 particles that activates into cloud drops at any given S_{eff} , the difference in how S_{eff} affects A at
12 all examined locations diminishes. In Hyytiälä, Vavihill and Jungfraujoch particles with a dry
13 diameter of 100 nm activate at the S_{eff} of slightly higher than 0.2% assuming an internally mixed
14 aerosol. Around this S_{eff} Mace Head does exhibit a slightly higher A_{100} compared to other
15 locations, possibly due to the increased CCN activity of the organically-enriched Aitken mode
16 aerosol (Ovadnevaite et al., 2011).

17 When A_{50} is examined in detail, the difference between Mace Head and other locations seen in
18 Figure 4 remains, with Mace Head exhibiting a higher activated fraction compared to the three
19 other locations. In Hyytiälä, Vavihill and Jungfraujoch particles with a dry diameter of 50 nm
20 activate at a S_{eff} of ~0.7%, while in Mace Head these same particles activate at a S_{eff} of ~0.55%.
21 Differences observed in Figures 4 and 5 lead to the conclusion that A_{50} and A_{100} have a more
22 stable dependence on S ; i.e. the variability in the fraction of nucleation/Aitken mode particles
23 among different locations is large. Consequently, when comparing datasets of activated
24 fractions A from several locations with different expected concentrations of nucleation/Aitken
25 mode particles and instrumental setups, a recommendation is made for the consideration of
26 using N_{100} and/or N_{50} concentrations instead of N_{CN} when calculating A coupled with A values
27 derived from total number concentrations. Besides more systematic comparison of activation
28 curves and, therefore, more accurate results, such an approach can provide additional
29 information about the effect of size distribution and its variability, and hygroscopicity on CCN
30 activation. The use of A_{100} and A_{50} also diminishes the effect of the spatial variability of the
31 fraction of nucleation/Aitken mode particles, those less relevant for CCN activation at typical
32 ambient S_{eff} levels.

1 **3.3 CCN and their hygroscopicity**

2 Critical dry diameter D_c and hygroscopicity parameter κ were provided for the majority of the
3 presented locations, and the variation of κ with dry size is seen in Figure 6 (the figure is split
4 into four panels for better visual representation). The variation of κ with dry size is not the same
5 everywhere, and three groups can be pointed out.

6 In the first group of locations κ clearly increases with size; this is the case for Hyytiälä, Vavihill,
7 Jungfraujoch (Figure 6, upper left panel), Pallas (Figure 6, upper right panel), and for the four
8 campaigns conducted by the MPIC (Figure 6, lower right panel). At these locations
9 accumulation mode particles have a higher hygroscopicity than the Aitken mode particles,
10 likely due to cloud processing. The results of the Mann-Whitney U test (Mann and Whitney,
11 1947) for two populations that are not normally distributed (below and above 100 nm of dry
12 size; Paramonov et al., 2013) reveal that in Hyytiälä, Vavihill, Jungfraujoch and Pallas A and
13 C the difference in κ is statistically significant at the 5% significance level, i.e. the median κ of
14 Aitken and accumulation mode particles are significantly different (Table 5). Published data
15 for the PRIDE-PRD2006, CAREBeijing-2006, CLACE-6 and AMAZE-08 campaigns have
16 previously reported such a trend (Rose et al., 2010; Gunthe et al., 2011; Rose et al., 2013;
17 Gunthe et al., 2009, respectively). Data for Chilbolton (Figure 6, lower left panel) also reveal
18 an increase in κ with size, although absolute κ values at this site may be underestimated due to
19 the aerosol sample not being dried before entering the CCNC (Whitehead et al., 2014). Such
20 behaviour of κ leads to two implications. First, as already discussed in Su et al. (2010) and
21 Paramonov et al. (2013), the hygroscopicity of the whole aerosol population can, and in some
22 cases should, be presented as a function of size; this can be done by way of either separate κ
23 values for the Aitken and accumulation mode aerosol or hygroscopicity distribution functions.
24 Values of κ derived from the CCNC are frequently discussed in conjunction with the chemistry
25 information obtained, e.g. from the Aerosol Mass Spectrometer (AMS) measurements. The
26 second implication here is that if, due to instrumental limitations, such measurements are
27 representative only of the accumulation mode particles, κ values derived from such
28 measurements should be extended to the Aitken mode particles with caution. The effect of
29 extending the accumulation mode κ down to the Aitken mode was examined using detailed data
30 from Hyytiälä as an example. N_{CCN} was calculated using the median annual size distribution
31 and D_c calculated with size-dependent and the assumed size-independent κ values. It was found

1 that if κ of the accumulation mode is assumed to be the same for the Aitken mode, the N_{CCN} , on
2 average, is overestimated by 16% and 13.5% for the S_{eff} of 0.6% and 1.0%, respectively.

3 The second group of locations, or in this case only one location, exhibits a decrease of κ with
4 particle dry size, and such a trend exists only for the COPS campaign (Figure 6, lower left
5 panel). Apparently, at the mountainous site in the Black Forest region of south-west Germany
6 the chemical composition of the accumulation mode aerosol makes it less hygroscopic
7 compared with the Aitken mode at supersaturated conditions (Irwin et al., 2011). However, the
8 same study reported that the measurements by the Hygroscopicity Tandem DMA (HTDMA) in
9 a sub-saturated regime revealed an increase of κ with particle dry size.

10 The third group of locations, represented by the K-pusztá station and RHaMBLe measurement
11 campaign, is characterised by the absence of any dependence of κ on the particle dry size.
12 Though quite different in magnitude (Figure 6, lower left panel), κ values and, therefore, aerosol
13 chemical composition seem to have no particular size dependence across the whole measured
14 size range. Also of interest is the high aerosol hygroscopicity across the whole investigated
15 aerosol size range (Aitken mode) during the RHaMBLe cruise – all κ values are just below
16 unity (Good et al., 2010). The marine nature of the aerosol and clean background conditions of
17 the remote tropical North Atlantic are likely responsible for high aerosol hygroscopicity.

18 Three of the four long-term datasets, excluding Mace Head, included D_c and κ data, making it
19 possible to examine aerosol hygroscopicity both on the annual basis and diurnal basis separated
20 by seasons. Figure 7 presents the annual variation of D_c for lowest and highest S_{eff} levels in
21 Hyytiälä, Vavihill and Jungfraujoch. As can be seen in the y -axis of the upper panel, particles
22 measured at the S_{eff} of 0.1% are in the accumulation mode, i.e. D_c is larger than 100 nm in
23 diameter. Of the three stations presented, D_c has an annual pattern only in Hyytiälä, with a
24 minimum D_c and an increased hygroscopicity in the winter and a maximum D_c and a decreased
25 hygroscopicity in the summer, as previously reported by Paramonov et al. (2013). The likely
26 reason for a decrease in the accumulation mode particle hygroscopicity in Hyytiälä in the
27 summer is the increase in the emissions of the volatile organic compounds (VOCs), leading to
28 an increase in secondary organic aerosol (SOA) formation and, thus, a higher organic fraction.
29 The higher hygroscopicity in the winter can also be explained by a higher sulphate fraction,
30 stronger aerosol oxidation and potentially other aging processes which are known to increase
31 particle hygroscopicity (Furutani et al., 2008). No annual pattern is present in the aerosol
32 hygroscopicity of accumulation mode aerosol in Vavihill and Jungfraujoch. The lower panel in

1 Figure 7 depicts the annual variation of aerosol hygroscopicity for the Aitken mode aerosol,
2 revealing no pattern for any of the three locations. The absence of a pattern coupled with the
3 absence of an apparent difference among sites indicates that the aerosol hygroscopicity of
4 Aitken, ~50 nm aerosol is fairly similar and constant throughout the year at all three locations.
5 The diurnal patterns of aerosol hygroscopicity were analysed for Hyytiälä, Vavihill and
6 Jungfraujoch on a seasonal basis. It was discovered that for the accumulation mode particles,
7 those measured at the S_{eff} of 0.1%, no diurnal pattern was observed at any of the three locations
8 in any of the seasons, indicating that throughout the day photochemistry does not have any
9 apparent effect on the hygroscopicity of the accumulation mode particles. Diurnal patterns of
10 aerosol hygroscopicity for Aitken mode particles can be seen in Figure 8. In the winter no
11 particular pattern is visible at any of the locations; it can, however, be seen that while the aerosol
12 hygroscopicity is similar between Hyytiälä and Vavihill, the Aitken mode aerosol at the
13 Jungfraujoch is less hygroscopic. In the spring both Hyytiälä and Vavihill exhibit a clear diurnal
14 pattern, which extends also into the summer. A peak in aerosol hygroscopicity is observed
15 around midday when D_c reaches its minimum. Several previous studies have reported such
16 behaviour in Hyytiälä and have attributed it to the vegetation activity, photochemistry and the
17 aging of organics during the sunlight hours (Sihto et al., 2011; Cerully et al., 2011; Paramonov
18 et al., 2013). While no diurnal pattern of aerosol hygroscopicity is visible for Jungfraujoch for
19 winter and spring, a very clear pattern does exist in the summer and autumn. In these seasons
20 Aitken mode particles exhibit an obvious decrease in hygroscopicity in the afternoon shown by
21 the peak in D_c during these hours. This phenomenon has also been previously reported and
22 attributed to the daytime intrusions of air from the planetary boundary layer (PBL) injecting
23 less hygroscopic particles into the free troposphere (Kammermann et al., 2010a). The
24 discussion above demonstrates that diurnal patterns of hygroscopicity are not the same
25 everywhere and vary by seasons; however, the environments of Hyytiälä and Vavihill are
26 similar enough to result in similar diurnal patterns.

27

28 **4 Conclusion**

29 CCNC measurement data from 14 locations, including four long-term measurement sites, have
30 been analysed, compared and discussed with respect to the deduced CCN activation and
31 hygroscopic properties. As already known, the pattern of how N_{CCN} and A respond to the
32 increasing S is indicative of the total N_{CN} concentrations, the size distribution of the pre-existing

1 aerosol population and its hygroscopicity. Certain marine locations exhibited high A values and
2 rapidly increasing N_{CCN} even at low S values, as was the case during the COPS campaign in
3 south-west Germany. At these locations aerosol populations are likely accumulation mode-
4 dominated and/or of relatively high hygroscopicity. Pallas, a remote background location in
5 northern Finland, exhibited a pattern of low A values and slowly increasing N_{CCN} at low S
6 values, revealing the likelihood of Aitken mode-dominated aerosol and/or fairly low
7 hygroscopicity at this site. Jungfraujoch, a high Alpine site in the free troposphere, also
8 exhibited comparatively low A values, as the particle number is often dominated by the Aitken
9 mode particles. For the rest of the studied locations, the majority, the pattern of increasing A
10 with increasing S was similar, i.e. at most locations the same fraction of aerosol activated into
11 cloud drops at any given S . For example, 20% of the total aerosol population at most locations
12 will activate into cloud drops at the S of 0.1%. A simple linear fit for estimating annual mean
13 N_{CCN} at most continental locations is presented. When comparing activated fractions A at
14 several locations, a recommendation is made to use N_{100} and/or N_{50} when calculating A values
15 together with A values derived from total number concentrations. Using this technique, a more
16 accurate comparison should be performed for sites where the exact size range of N_{CN} is not
17 known and where the concentrations of nucleation/Aitken mode particles are expected to be
18 high, additionally revealing more information about the effect of size distribution and
19 hygroscopicity on CCN activation.

20 The hygroscopicity of aerosol particles as a function of size is not the same at all locations;
21 while κ decreased with increasing size at a continental site in south-west Germany and was
22 fluctuating without any particular size dependence across the observed size range in the remote
23 tropical North Atlantic and rural central Hungary, all other locations exhibited an increase of κ
24 with size. In fact, at the rural background sites of southern Finland and southern Sweden, at a
25 free troposphere site in the Swiss Alps and at a remote background site in northern Finland the
26 difference in hygroscopicity between Aitken and accumulation mode aerosol was statistically
27 significant at the 5% significance level. Therefore, assuming a size-independent κ can lead to a
28 substantial overestimation of N_{CCN} at higher levels of S_{eff} (those above 0.6%). The
29 hygroscopicity of the whole aerosol population can be presented separately for Aitken and
30 accumulation mode particles; additionally, hygroscopicity distribution functions can be used to
31 analyse size-resolved CCNC data and efficiently describe the size dependence of κ (Lance,
32 2007; Su et al., 2010; Jurányi et al., 2013). It is known, however, that in most cases the size

1 distribution and its variation have a larger effect on the N_{CCN} than the particle hygroscopicity
2 and its variation with size.

3 Among Hyytiälä, Vavihill and Jungfraujoch, no annual pattern of aerosol hygroscopicity was
4 found for the Aitken mode aerosol. The accumulation mode aerosol exhibited a discernible
5 annual pattern only in Hyytiälä, where a peak in hygroscopicity was found in February and a
6 minimum in July. Such a pattern is likely attributed to the higher sulphate fraction and stronger
7 aerosol oxidation in the winter and active SOA formation and higher organic fraction in the
8 summer. Among the same three sites, no diurnal trend of aerosol hygroscopicity was found for
9 accumulation mode aerosol. The hygroscopicity of the Aitken mode aerosol in Hyytiälä and
10 Vavihill follows a clear diurnal pattern in the spring and summer – an increase in aerosol
11 hygroscopicity was observed in the afternoon, likely due to the photochemistry and aging of
12 the organics. At the Jungfraujoch, Aitken mode aerosol showed a decrease in aerosol
13 hygroscopicity in the afternoon during the summer and autumn; this phenomenon is caused by
14 the injections from the planetary boundary layer containing somewhat less hygroscopic aerosol.

15 In general, the comparison of CCNC measurements is complicated by the variation of
16 instrumental setups, settings, measurement times and intervals, performed calibrations,
17 calculations and available parameters among sites. Supplementary data, such as aerosol size
18 distribution and chemical composition, can enhance the uniformity of the analysis and expand
19 the representativeness of the aforementioned results. However, as the first overview of its kind,
20 the summary of CCNC measurements discussed here presents a unique insight into the CCN
21 activation and hygroscopic properties in Europe and a few non-European sites. While, as shown
22 here, CCNC measurements can provide useful information about the CCN and their activation
23 into cloud droplets, the missing link in the aerosol-cloud interactions is the connection of CCN
24 to the ambient CDNC. If filled, this gap can greatly improve our understanding of the processes
25 and feedbacks within the aerosol-cloud-climate triangle and enhance the performance and
26 accuracy of the global climate models.

27

28 **Acknowledgements**

29 The research leading to the results published herein has received funding from the ACTRIS
30 Project of the European Union Seventh Framework Programme (FP7/2007-2013) under grant
31 agreement n° 262254. Additional funding was provided by the Max Planck Society. HEA-
32 PRTL14 Environment and Climate: Impact and Responses programme, EC 6th Framework

1 programme project EUCAARI (036833-2), EC 7th Framework programme project BACCHUS
2 (603445) are all acknowledged. The authors would like to thank Jakub Bialek for collecting
3 CCN data and Ciaran Monahan for SMPS measurements at Mace Head station. The authors
4 would also like to thank Dr. Tuomo Nieminen and Dr. Ari Asmi for the help with statistics and
5 data analysis. Simon Schallhart, Ksenia Atlaskina and Anna Nikandrova are all gratefully
6 acknowledged for the discussions, help and support with the data analysis and plotting. The
7 Centre of Excellence in Atmospheric Science – from molecular and biological processes to the
8 global climate FCoE, Cryosphere-atmosphere interactions in a changing Arctic climate
9 CRAICC initiative and KONE foundation are acknowledged as well. The measurements at the
10 Jungfrauoch were supported by MeteoSwiss in the framework of the Global Atmosphere
11 Watch programme and the infrastructure was supported by the International Foundation High
12 Altitude Research Station Jungfrauoch and Gornergrat. M.G. was supported by the ERC under
13 grant 615922-BLACARAT.

14

15 **References**

16 Andreae, M. O.: Correlation between cloud condensation nuclei concentration and aerosol
17 optical thickness in remote and polluted regions, *Atmos. Chem. Phys.*, 9, 543–556, 2009.

18 Andreae, M. O. and Rosenfeld, D.: Aerosol-cloud-precipitation interactions. Part 1. The nature
19 and sources of cloud-active aerosols, *Earth-Sci. Rev.*, 89, 13–41,
20 doi:10.1016/j.earscirev.2008.03.001, 2008.

21 Asmi, A., Wiedensohler, A., Laj, P., Fjaeraa, A.-M., Sellegri, K., Birmili, W., Weingartner, E.,
22 Baltensperger, U., Zdimal, V., Zikova, N., Putaud, J.-P., Marinoni, A., Tunved, P., Hansson,
23 H.-C., Fiebig, M., Kivekäs, N., Lihavainen, H., Asmi, E., Ulevicius, V., Aalto, P. P., Swietlicki,
24 E., Kristensson, A., Mihalopoulos, N., Kalivitis, N., Kalapov, I., Kiss, G., de Leeuw, G.,
25 Henzing, B., Harrison, R. M., Beddows, D., O'Dowd, C., Jennings, S. G., Flentje, H., Weinhold,
26 K., Meinhardt, F., Ries, L., and Kulmala, M.: Number size distributions and seasonality of
27 submicron particles in Europe 2008–2009, *Atmos. Chem. Phys.*, 11, 5505–5538,
28 doi:10.5194/acp-11-5505-2011, 2011.

29 Beddows, D. C. S., Dall'Osto, M., Harrison, R. M., Kulmala, M., Asmi, A., Wiedensohler, A.,
30 Laj, P., Fjaeraa, A. M., Sellegri, K., Birmili, W., Bukowiecki, N., Weingartner, E.,
31 Baltensperger, U., Zdimal, V., Zikova, N., Putaud, J.-P., Marinoni, A., Tunved, P., Hansson,

1 H.-C., Fiebig, M., Kivekäs, N., Swietlicki, E., Lihavainen, H., Asmi, E., Ulevicius, V., Aalto,
2 P. P., Mihalopoulos, N., Kalivitis, N., Kalapov, I., Kiss, G., de Leeuw, G., Henzing, B.,
3 O'Dowd, C., Jennings, S. G., Flentje, H., Meinhardt, F., Ries, L., Denier van der Gon, H. A. C.,
4 and Visschedijk, A. J. H.: Variations in tropospheric submicron particle size distributions across
5 the European continent 2008–2009, *Atmos. Chem. Phys.*, 14, 4327–4348, 10.5194/acp-14-
6 4327-2014, 2014.

7 Bègue, N.: Evolution des propriétés physico-chimiques des aérosols désertiques issus de
8 l'outflow africain, *Ocean, Atmosphere*, Université de la Réunion, Saint-Denis, Réunion,
9 France, 2012.

10 Boucher, O., and Lohmann, U.: The sulfate-CCN-cloud albedo effect, *Tellus*, 47B, 281–300,
11 1995.

12 Boucher, O., Randall, D., Artaxo, P., Bretherton, C., Feingold, G., Forster, P., Kerminen, V.-
13 M., Kondo, Y., Liao, H., Lohmann, U., Rasch, P., Satheesh, S. K., Sherwood, S., Stevens, B.,
14 and Zhang, X. Y.: Clouds and aerosols, in: *Climate Change 2013: The Physical Science Basis*,
15 Contribution of Working Group I to the Fifth Assessment Report of the Intergovernmental
16 Panel on Climate Change, edited by: Stocker, T. F., Qin, D., Plattner, G.-K., Tignor, M., Allen,
17 S. K., Boschung, J., Nauels, A., Xia, Y., Bex, V., and Midgley, P. M., Cambridge University
18 Press, Cambridge, UK and New York, NY, USA, 571–657, 2013.

19 Bougiatioti, A., Fountoukis, C., Kalivitis, N., Pandis, S. N., Nenes, A., and Mihalopoulos, N.:
20 Cloud condensation nuclei measurements in the marine boundary layer of the eastern
21 Mediterranean: CCN closure and droplet growth kinetics, *Atmos. Chem. Phys.*, 9, 7053–7066,
22 2009.

23 Brus, D., Neitola, K., Asmi, E., Aurela, M., Makkonen, U., Svensson, J., Hyvärinen, A.-P.,
24 Hirsikko, A., Hakola, H., Hillamo, R., and Lihavainen, H.: Pallas cloud experiment, PACE
25 2012, *AIP Conf. Proc.*, 1527, 964, doi:10.1063/1.4803433, 2013.

26 Campanelli, M., Estelles, V., Smyth, T., Tomasi, C., Martínez-Lozano, M. P., Claxton, B.,
27 Muller, P., Pappalardo, G., Pietruczuk, A., Shanklin, J., Colwell, S., Wrench, C., Lupi, A.,
28 Mazzola, M., Lanconelli, C., Vitale, V., Congeduti, F., Dionisi, D., Cardillo, F., Cacciani, M.,
29 Casasanta, G., and Nakajima, T.: Monitoring of Eyjafjallajökull volcanic aerosol by the new
30 European Skynet Radiometers (ESR) network, *Atmos. Environ.*, 48, 33–45, 2012.

1 Carrico, M. C., Petters, M. D., Kreidenweis, S. M., Collett Jr., J. L., Engling, G., and Malm, W.
2 C.: Aerosol hygroscopicity and cloud droplet activation of extracts of filters from biomass
3 burning experiments, *J. Geophys. Res.*, 113, D08206, doi:10.1029/2007JD009274, 2008.

4 Cerully, K. M., Raatikainen, T., Lance, S., Tkacik, D., Tiitta, P., Petäjä, T., Ehn, M., Kulmala,
5 M., Worsnop, D. R., Laaksonen, A., Smith, J. N., and Nenes, A.: Aerosol hygroscopicity and
6 CCN activation kinetics in a boreal forest environment during the 2007 EUCAARI campaign,
7 *Atmos. Chem. Phys.*, 11, 12369–12386, 2011.

8 Chang, R. Y.-W., Liu, P. S. K., Leaitch, W. R., and Abbatt, J. P. D.: Comparison between
9 measured and predicted CCN concentrations at Egbert, Ontario: Focus on the organic aerosol
10 fraction at a semi-rural site, *Atmos. Environ.*, 41, 8172–8182, 2007.

11 Chen, Y.-C., Christensen, M. W., Stephens, G. L., and Seinfeld, J. H.: Satellite-based estimate
12 of global aerosol-cloud radiative forcing by marine warm clouds, *Nat. Geosci.*, 7, 643–646,
13 2014.

14 Collaud Coen, M., Weingartner, E., Furger, M., Nyeki, S., Prévôt, A. S. H., Steinbacher, M.,
15 and Baltensperger, U.: Aerosol climatology and planetary boundary influence at the
16 Jungfraujoch analyzed by synoptic weather types, *Atmos. Chem. Phys.*, 11, 5931–5944, 2011.

17 Covert, D. S., Gras, J. L., Wiedensohler, A., and Stratmann, F.: Comparison of directly
18 measured CCN with CCN modeled from the number-size distribution in the marine boundary
19 layer during ACE 1 at Cape Grim, Tasmania, *J. Geophys. Res.*, 103, D13, 16597–16608, 1998.

20 Ditas, F., Shaw, R. A., Siebert, H., Simmel, M., Wehner, B., and Wiedensohler, A.: Aerosol-
21 cloud microphysics-thermodynamics-turbulence: evaluating supersaturation in a marine
22 stratocumulus cloud, *Atmos. Chem. Phys.*, 12, 2459–2468, doi:10.5194/acp-12-2459-2012,
23 2012.

24 Dusek, U., Frank, G. P., Hildebrandt, L., Curtius, J., Schneider, J., Walter, S., Chand, D.,
25 Drewnick, F., Hings, S., Jung, D., Borrmann, S., and Andreae, M. O.: Size matters more than
26 chemistry for cloud-nucleating ability of aerosol particles, *Science*, 312, 1375–1378,
27 doi:10.1126/science.1125261, 2006.

28 Facchini, M. C., Decesari, S., Mircea, M., Fuzzi, S., and Loglio, G.: Surface tension of
29 atmospheric wet aerosol and cloud/fog droplets in relation to their organic carbon content and
30 chemical composition, *Atmos. Environ.*, 34, 4853–4857, 2000.

- 1 Fors, E. O., Swietlicki, E., Svenningsson, B., Kristensson, A., Frank, G. P., and Sporre, M.:
2 Hygroscopic properties of the ambient aerosol in southern Sweden – a two year study, *Atmos.*
3 *Chem. Phys.*, 11, 8343–8361, 2011.
- 4 Furutani, H., Dall’osto, M., Roberts, G. C., and Prather, K. A.: Assessment of the relative
5 importance of atmospheric aging on CCN activity derived from field observations, *Atmos.*
6 *Environ.*, 42, 3130–3142, 2008.
- 7 Garland, R. M., Schmid, O., Nowak, A., Achtert, P., Wiedensohler, A., Gunthe, S. S.,
8 Takegawa, N., Kita, K., Kondo, Y., Hu, M., Shao, M., Zeng, M., Zhu, T., Andreae, M. O., and
9 Pöschl, U.: Aerosol optical properties observed during Campaign of Air Quality Research in
10 Beijing 2006 (CAREBeijing-2006): Characteristic differences between the inflow and outflow
11 of Beijing city air, *J. Geophys. Res.*, 114, D00G04, doi: 10.1029/2008JD010780, 2009.
- 12 Good, N., Topping, D. O., Allan, J. D., Flynn, M., Fuentes, E., Irwin, M., Williams, P. I., Coe,
13 H., and McFiggans, G.: Consistency between parameterisations of aerosol hygroscopicity and
14 CCN activity during the RHaMBLe discovery cruise, *Atmos. Chem. Phys.*, 10, 3189–3203,
15 2010.
- 16 Gunthe, S. S., King, S. M., Rose, D., Chen, Q., Roldin, P., Farmer, D. K., Jimenez, J. L., Artaxo,
17 P., Andreae, M. O., Martin, S. T., and Pöschl, U.: Cloud condensation nuclei in pristine tropical
18 rainforest air of Amazonia: size-resolved measurements and modeling of atmospheric aerosol
19 composition and CCN activity, *Atmos. Chem. Phys.*, 9, 7551-7575, 2009.
- 20 Gunthe, S. S., Rose, D., Su, H., Garland, R. M., Achtert, P., Nowak, A., Wiedensohler, A.,
21 Kuwata, M., Takegawa, N., Kondo, Y., Hu, M., Shao, M., Zhu, T., Andreae, M. O., and Pöschl,
22 U.: Cloud condensation nuclei (CCN) from fresh and aged air pollution in the megacity region
23 of Beijing, *Atmos. Chem. Phys.*, 11, 11023–11039, 2011.
- 24 Hammer, E., Bukowiecki, N., Gysel, M., Jurányi, Z., Hoyle, C. R., Vogt, R., Baltensperger, U.,
25 and Weingartner, E.: Investigation of the effective peak supersaturation for liquid-phase clouds
26 at the high-alpine site Jungfrauoch, Switzerland, *Atmos. Chem. Phys.*, 14, 1123–1139,
27 doi:10.5194/acp-14-1123-2014, 2014.
- 28 Hari, P. and Kulmala, M.: Station for Measuring Ecosystem–Atmosphere Relations (SMEAR
29 II), *Boreal Environ. Res.*, 10, 315–322, 2005.

1 Hatakka, J., Aalto, T., Aaltonen, V., Aurela, M., Hakola, H., Komppula, M., Laurila, T.,
2 Lihavainen, H., Paatero, J., Salminen, K., and Viisanen, Y.: Overview of the atmospheric
3 research activities and results at Pallas GAW station, *Boreal Environ. Res.*, 8, 365–384, 2003.

4 Hitzenberger, R., Giebl, H., Petzold, A., Gysel, M., Nyeki, S., Weingartner, E., Baltensperger,
5 U., and Wilson, C.W.: Properties of jet engine combustion particles during the PartEmis
6 experiment. Hygroscopic growth at supersaturated conditions, *Geophys. Res. Lett.*, 30, 1779,
7 doi:10.1029/2003GL017294, 2003.

8 Hudson, J. G. and Noble, S.: CCN and vertical velocity influences on droplet concentrations
9 and supersaturations in clean and polluted stratus clouds, *J. Atmos. Sci.*, 71, 312–331, 2014.

10 Hudson, J. G., Hallett, J., and Rogers, C. F.: Field and laboratory measurements of cloud-
11 forming properties of combustion aerosols, *J. Geophys. Res.*, 96, 10847-10859,
12 10.1029/91JD00790, 1991.

13 Ion, A. C., Vermeylen, R., Kourtchev, I., Cafmeyer, J., Chi, X., Gelencsér, A., Maenhaut, W.,
14 and Claeys, M.: Polar organic compounds in rural PM_{2.5} aerosols from K-Pusztá, Hungary,
15 during a 2003 summer field campaign: Sources and diel variations, *Atmos. Chem. Phys.*, 5,
16 1805–1814, 2005.

17 Irwin, M., Good, N., Crosier, J., Choulaton, T. W., and McFiggans, G.: Reconciliation of
18 measurements of hygroscopic growth and critical supersaturation of aerosol particles in central
19 Germany, *Atmos. Chem. Phys.*, 10, 11737–11752, doi:10.5194/acp- 10-11737-2010, 2010.

20 Jaatinen, A., Romakkaniemi, S., Anttila, T., Hyvärinen, A.-P., Hao, L.-Q., Kortelainen, A.,
21 Miettinen, P., Mikkonen, S., Smith, J. N., Virtanen, A., and Laaksonen, A.: The third Pallas
22 Cloud Experiment: Consistency between the aerosol hygroscopic growth and CCN activity,
23 *Boreal Environ. Res.*, 19 (suppl. B), 368–382, 2014.

24 Jones, H. M., Crosier, J., Russell, A., Flynn, M. J., Irwin, M., Choulaton, T. W., Coe, H., and
25 McFiggans, G.: In situ aerosol measurements taken during the 2007 COPS field campaign at
26 the Hornisgrinde ground site, *Q. J. R. Meteorol. Soc.*, 137, 252–266, 2011.

27 Jurányi, Z., Gysel, M., Weingartner, E., DeCarlo, P. F., Kammermann, L., and Baltensperger,
28 U.: Measured and modelled cloud condensation nuclei number concentration at the high alpine
29 site Jungfraujoch, *Atmos. Chem. Phys.*, 10, 7891–7906, 2010.

1 Jurányi, Z., Gysel, M., Weingartner, E., Bukowiecki, N., Kammermann, L., and Baltensperger,
2 U.: A 17 month climatology of the cloud condensation nuclei number concentration at the high
3 alpine site Jungfraujoch, *J. Geophys. Res.*, 116, D10204, doi:10.1029/2010JD015199, 2011.

4 Jurányi, Z., Tritscher, T., Gysel, M., Laborde, M., Gomes, L., Roberts, G., Baltensperger, U.,
5 and Weingartner, E.: Hygroscopic mixing state of urban aerosol derived from size-resolved
6 cloud condensation nuclei measurements during the MEGAPOLI campaign in Paris, *Atmos.*
7 *Chem. Phys.*, 13, 6431–6446, 2013.

8 Kammermann, L., Gysel, M., Weingartner, E., and Baltensperger, U.: 13-month climatology of
9 the aerosol hygroscopicity at the free tropospheric site Jungfraujoch (3580 m a.s.l.), *Atmos.*
10 *Chem. Phys.*, 10, 10717–10732, 2010a.

11 Kammermann, L., Gysel, M., Weingartner, E., Herich, H., Cziczo, D. J., Holst, T.,
12 Svenningsson, B., Arneth, A., and Baltensperger, U.: Subarctic atmospheric aerosol
13 composition: 3. Measured and modeled properties of cloud condensation nuclei, *J. Geophys.*
14 *Res.*, 115, D04202, doi:10.1029/2009JD012447, 2010b.

15 Kerminen, V.-M., Paramonov, M., Anttila, T., Riipinen, I., Fountoukis, C., Korhonen, H.,
16 Asmi, E., Laakso, L., Lihavainen, H., Swietlicki, E., Svenningsson, B., Asmi, A., Pandis, S. N.,
17 Kulmala, M., and Petäjä, T.: Cloud condensation nuclei production associated with atmospheric
18 nucleation: a synthesis based on existing literature and new results, *Atmos. Chem. Phys.*, 12,
19 12037–12059, 2012.

20 Khvorostyanov, V. I. and Curry, J. A.: Refinements to the Köhler's theory of aerosol
21 equilibrium radii, size spectra, and droplet activation: Effects of humidity and insoluble
22 fraction, *J. Geophys. Res.*, 112, D05206, doi:10.1029/2006JD007672, 2007.

23 Knutson, E. O., and Whitby, K. T.: Aerosol classification by electric mobility: apparatus, theory
24 and applications, *J. Aerosol Sci.*, 6, 443–451, 1975.

25 Köhler, H.: The nucleus in and the growth of hygroscopic droplets, *T. Faraday Soc.*, 32, 1152–
26 1161, 1936.

27 Komppula, M., Sihto, S.-L., Korhonen, H., Lihavainen, H., Kerminen, V.-M., Kulmala, M., and
28 Viisanen, Y.: New particle formation in air mass transported between two measurement sites
29 in northern Finland, *Atmos. Chem. Phys.*, 6, 2811–2824, 2006.

1 Kuang, C., McMurry, P. H., and McCormick, A. V.: Determination of cloud condensation
2 nuclei production from measured new particle formation events, *Geophys. Res. Lett.*, 36,
3 L09822, doi:10.1029/2009GL037584, 2009.

4 Kulmala, M., Korhonen, P., Vesala, T., Hansson, H.-C., Noone, K., and Svenningsson, B.: The
5 effect of hygroscopicity on cloud droplet formation, *Tellus B*, 48, 347–360, 1996.

6 Kulmala, M., Asmi, A., Lappalainen, H. K., Baltensperger, U., Brenguier, J.-L., Facchini, M.
7 C., Hansson, H.-C., Hov, Ø., O’Dowd, C. D., Pöschl, U., Wiedensohler, A., Boers, R., Boucher,
8 O., de Leeuw, G., Denier van den Gon, H., Feichter, J., Krejci, R., Laj, P., Lihavainen, H.,
9 Lohmann, U., McFiggans, G., Mentel, T., Pilinis, C., Riipinen, I., Schulz, M., Stohl, A.,
10 Swietlicki, E., Vignati, E., Alves, C., Amann, M., Ammann, M., Arabas, S., Artaxo, P., Baars,
11 H., Beddows, D. C. S., Bergström, R., Beukes, J. P., Bilde, M., Burkhardt, J. F., Canonaco, F.,
12 Clegg, S., Coe, H., Crumeyrolle, S., D’Anna, B., Decesari, S., Gilardoni, S., Fischer, M.,
13 Fjærraa, A. M., Fountoukis, C., George, C., Gomes, L., Halloran, P., Hamburger, T., Harrison,
14 R. M., Herrmann, H., Hoffmann, T., Hoose, C., Hu, M., Hyvärinen, A., Hörrak, U., Iinuma, Y.,
15 Iversen, T., Josipovic, M., Kanakidou, M., Kiendler-Scharr, A., Kirkevåg, A., Kiss, G.,
16 Klimont, Z., Kolmonen, P., Komppula, M., Kristjansson, J.-E., Laakso, L., Laaksonen, A.,
17 Labonnote, L., Lanz, V. A., Lehtinen, K. E. J., Rizzo, L. V., Makkonen, R., Manninen, H. E.,
18 McMeeking, G., Merikanto, J., Minikin, A., Mirme, S., Morgan, W. T., Nemitz, E., O’Donnell,
19 D., Panwar, T. S., Pawlowska, H., Petzold, A., Pienaar, J. J., Pio, C., Plass-Duelmer, C., Prévôt,
20 A. S. H., Pryor, S., Reddington, C. L., Roberts, G., Rosenfeld, D., Schwarz, J., Seland, Ø.,
21 Sellegri, K., Shen, X. J., Shiraiwa, M., Siebert, H., Sierau, B., Simpson, D., Sun, J. Y., Topping,
22 D., Tunved, P., Vaattovaara, P., Vakkari, V., Veefkind, J. P., Visschedijk, A., Vuollekoski, H.,
23 Vuolo, R., Wehner, B., Wildt, J., Woodward, S., Worsnop, D. R., van Zadelhoff, G.-J., Zardini,
24 A. A., Zhang, K., van Zyl, P. G., Kerminen, V.-M., Carslaw, K. S., and Pandis, S. N.: General
25 overview: European Integrated project on Aerosol Cloud Climate and Air Quality interactions
26 (EUCAARI) – integrating aerosol research from nano to global scales, *Atmos. Chem. Phys.*,
27 11, 13061–13143, 2011.

28 Laaksonen, A., Hamed, A., Joutsensaari, J., Hiltunen, L., Cavalli, F., Junkermann, W., Asmi,
29 A., Fuzzi, S., and Facchini, M. C.: Cloud condensation nucleus production from nucleation
30 events at a highly polluted region, *Geophys. Res. Lett.*, 32, L06812,
31 doi:10.1029/2004GL022092, 2005.

1 Lance, S.: Quantifying compositional impacts of ambient aerosol on cloud droplet formation,
2 Ph.D. thesis, Georgia Institute of Technology, Atlanta GA, USA, 166 pp., 2007.

3 Levin, E. J. T., Prenni, A. J., Palm, B. B., Day, D. A., Campuzano-Jost, P., Winkler, P. M.,
4 Kreidenweis, S. M., DeMott, P. J., Jimenez, J. L., and Smith, J. N.: Size-resolved aerosol
5 composition and its link to hygroscopicity at a forested site in Colorado, *Atmos. Chem. Phys.*,
6 14, 2657–2667, 2014.

7 Mann, H. B., and Whitney, D. R.: On a test of whether one of two random variables is
8 stochastically larger than the other, *Ann. Math. Stat.*, 18(1), 50–60, 1947.

9 Martin, S. T., Andreae, M. O., Althausen, D., Artaxo, P., Baars, H., Borrmann, S., Chen, Q.,
10 Farmer, D. K., Guenther, A., Gunthe, S., Jimenez, J. L., Karl, T., Longo, K., Manzi, A.,
11 Pauliquevis, T., Petters, M., Prenni, A., Pöschl, U., Rizzo, L. V., Schneider, J., Smith, J. N.,
12 Swietlicki, E., Tota, J., Wang, J., Wiedensohler, A., and Zorn, S. R.: An overview of the
13 Amazonian Aerosol Characterization Experiment 2008 (AMAZE-08), *Atmos. Chem. Phys.*,
14 10, 11415–11438, 2010.

15 Mason, B. J., and Chien, C. W.: Cloud-droplet growth by condensation in cumulus, *Q. J. Roy.*
16 *Meteor. Soc.*, 88, 136–142, 1962.

17 McFiggans, G., Artaxo, P., Baltensperger, U., Coe, H., Facchini, M. C., Feingold, G., Fuzzi, S.,
18 Gysel, M., Laaksonen, A., Lohmann, U., Mentel, T. F., Murphy, D. M., O’Dowd, C. D., Snider,
19 J. R., and Weingartner, E.: The effect of physical and chemical aerosol properties on warm
20 cloud droplet activation, *Atmos. Chem. Phys.*, 6, 2593–2649, 2006.

21 Mensah, A. A., Holzinger, R., Otjes, R., Trimborn, A., Mentel, Th. F., ten Brink, H., Henzing,
22 B., and Kiendler-Scharr, A.: Aerosol chemical composition at Cabauw, The Netherlands as
23 observed in two intensive periods in May 2008 and March 2009, *Atmos. Chem. Phys.*, 12,
24 4723–4742, 2012.

25 Moore, R. H., Karydis, V. A., Capps, S. L., Latham, T. L., and Nenes, A.: Droplet number
26 uncertainties associated with CCN: an assessment using observations and a global model
27 adjoint, *Atmos. Chem. Phys.*, 13, 4235–4251, 2013.

28 Morales Betancourt, R., and Nenes, A.: Understanding the contributions of aerosol properties
29 and parameterization discrepancies to droplet number variability in a global climate model,
30 *Atmos. Chem. Phys.*, 14, 4809–4826, doi:10.5194/acp-14-4809-2014, 2014.

1 O'Dowd, C., Ceburnis, D., Ovadnevaite, J., Vaishya, A., Rinaldi, M., and Facchini, M. C.: Do
2 anthropogenic, continental or coastal aerosol sources impact on a marine aerosol signature at
3 Mace Head?, *Atmos. Chem. Phys.*, 14, 10687–10704, 2014.

4 Ovadnevaite, J., Ceburnis, D., Martucci, G., Bialek, J., Monahan, C., Rinaldi, M., Facchini, M.
5 C., Berresheim, H., Worsnop, D. R., and O'Dowd, C.: Primary marine organic aerosol: A
6 dichotomy of low hygroscopicity and high CCN activity, *Geophys. Res. Lett.*, 38, L21806,
7 doi:10.1029/2011GL048869, 2011.

8 Pandis, S. N., Russell, L. M., and Seinfeld, J. H.: The relationship between DMS flux and CCN
9 concentration in remote marine regions, *J. Geophys. Res.*, 99, D8, 16945–16957, 1994.

10 Paramonov, M., Aalto, P. P., Asmi, A., Prisle, N., Kerminen, V.-M., Kulmala, M., and Petäjä,
11 T.: The analysis of size-segregated cloud condensation nuclei counter (CCNC) data and its
12 implications for cloud droplet activation, *Atmos. Chem. Phys.*, 13, 10285–10301, 2013.

13 Perry, K. D., Cliff, S. S., and Jimenez-Cruz, M. P.: Evidence for hygroscopic mineral dust
14 particles from the Intercontinental Transport and Chemical Transformation Experiment, *J.*
15 *Geophys. Res.*, 109, D23S28, doi:10.1029/2004JD004979, 2004.

16 Petters, M. D., and Kreidenweis, S. M.: A single parameter representation of hygroscopic
17 growth and cloud condensation nucleus activity, *Atmos. Chem. Phys.*, 7, 1961–1971, 2007.

18 Quinn, P. K., Bates, T. S., Coffman, D. J., and Covert, D. S.: Influence of particle size and
19 chemistry on the cloud nucleating properties of aerosols, *Atmos. Chem. Phys.*, 8, 1029–1042,
20 doi:10.5194/acp-8-1029-2008, 2008.

21 Ramanathan, V., Crutzen, P. J., Kiehl, J. T., and Rosenfeld, D.: Aerosols, climate, and the
22 hydrological cycle, *Science*, 294, 2119–2124, 2001.

23 Rissler, J., Pagels, J., Swietlicki, E., Wierzbicka, A., Strand, M., Lillieblad, L., Sanati, M., and
24 Bohgard, M.: Hygroscopic behavior of aerosol particles emitted from biomass fired grate
25 boilers, *Aerosol. Sci. Tech.*, 39, 919–930, doi:10.1080/02786820500331068, 2005.

26 Roberts, G. C. and Nenes, A.: A continuous-flow streamwise thermal-gradient CCN chamber
27 for atmospheric measurements, *Aerosol Sci. Tech.*, 39, 206–221,
28 doi:10.1080/027868290913988, 2005.

29 Rose, D., Gunthe, S. S., Mikhailov, E., Frank, G. P., Dusek, U., Andreae, M. O., and Pöschl,
30 U.: Calibration and measurement uncertainties of a continuous-flow cloud condensation nuclei

1 counter (DMT-CCNC): CCN activation of ammonium sulfate and sodium chloride aerosol
2 particles in theory and experiment, *Atmos. Chem. Phys.*, 8, 1153–1179, 2008.

3 Rose, D., Nowak, A., Achtert, P., Wiedensohler, A., Hu, M., Shao, M., Zhang, Y., Andreae, M.
4 O., and Pöschl, U.: Cloud condensation nuclei in polluted air and biomass burning smoke near
5 the mega-city Guangzhou, China – Part 1: Size-resolved measurements and implications for the
6 modeling of aerosol particle hygroscopicity and CCN activity, *Atmos. Chem. Phys.*, 10, 3365–
7 3383, 2010.

8 Rose, D., Gunthe, S. S., Jurányi, Z., Gysel, M., Frank, G. P., Schneider, J., Curtius, J., and
9 Pöschl, U.: Size-resolved and integral measurements of cloud condensation nuclei (CCN) at the
10 high-alpine site Jungfraujoch, *Atmos. Chem. Phys. Discuss.*, 13, 32575–32624, 2013.

11 Rosenfeld, D., Sherwood, S., Wood, R., and Donner, L.: Climate effects of aerosol-cloud
12 interactions, *Science*, 343, 379–380, 2014.

13 Seinfeld, J. H. and Pandis, S. N. (Eds.): *Atmospheric chemistry and physics: from air pollution
14 to climate change*, 2nd Edn., John Wiley & Sons, New York, USA, 2006.

15 Sihto, S.-L., Mikkilä, J., Vanhanen, J., Ehn, M., Liao, L., Lehtipalo, K., Aalto, P. P., Duplissy,
16 J., Petäjä, T., Kerminen, V.-M., Boy, M., and Kulmala, M.: Seasonal variation of CCN
17 concentrations and aerosol activation properties in boreal forest, *Atmos. Chem. Phys.*, 11,
18 13269–13285, 2011.

19 Snider, J. R., and Brenguier, J.-L.: Cloud condensation nuclei and cloud droplet measurements
20 during ACE-2, *Tellus*, 52B, 828–842, 2000.

21 Sogacheva, L., Dal Maso, M., Kerminen, V.-M., and Kulmala, M.: Probability of nucleation
22 events and aerosol particle concentration in different air mass types arriving at Hyytiälä,
23 southern Finland, based on back trajectories analysis, *Boreal Environ. Res.*, 10, 479–491, 2005.

24 Stock, M., Cheng, Y. F., Birmili, W., Massling, A., Wehner, B., Müller, T., Leinert, S.,
25 Kalivitis, N., Mihalopoulos, N., and Wiedensohler, A.: Hygroscopic properties of atmospheric
26 aerosol particles over the Eastern Mediterranean: implications for regional direct radiative
27 forcing under clean and polluted conditions, *Atmos. Chem. Phys.*, 11, 4251–4271, 2011.

28 Su, H., Rose, D., Cheng, Y. F., Gunthe, S. S., Massling, A., Stock, M., Wiedensohler, A.,
29 Andreae, M. O., and Pöschl, U.: Hygroscopicity distribution concept for measurement data

1 analysis and modeling of aerosol particle mixing state with regard to hygroscopic growth and
2 CCN activation, *Atmos. Chem. Phys.*, 10, 7489–7503, doi:10.5194/acp-10-7489-2010, 2010.

3 Svenningsson, I. B., Hansson, H. C., Wiedensohler, A., Ogren, J. A., Noone, K. J., and
4 Hallberg, A.: Hygroscopic growth of aerosol-particles in the Po Valley, *Tellus B*, 44(5), 556–
5 569, doi:10.1034/j.1600-0889.1992.t01-1-00009.x, 1992.

6 Topping, D.O.: Modelling the hygroscopic properties of atmospheric aerosols, Ph.D. thesis,
7 The University of Manchester, Manchester, UK, 257 pp., 2005.

8 Tunved, P., Hansson, H.-C., Kulmala, M., Aalto, P., Viisanen, Y., Karlsson, H., Kristensson,
9 A., Swietlicki, E., Dal Maso, M., Ström, J., and Komppula, M.: One year boundary layer aerosol
10 size distribution data from five Nordic background stations, *Atmos. Chem. Phys.*, 3, 2183–
11 2205, 2003.

12 Twomey, S.: The nuclei of natural cloud formation part II: The supersaturation in natural clouds
13 and the variation of cloud droplet concentration, *Geofisica pura e applicata*, 43(1), 243–249,
14 1959.

15 Vaillancourt, P. A., Yau, M. K., and Bartello, P.: Microscopic approach to cloud droplet growth
16 by condensation. Part II: Turbulence, clustering, and condensational growth, *J. Atmos. Sci.*, 59,
17 3421–3435, 2002.

18 Wang, J., Cubison, M. J., Aiken, A. C., Jimenez, J. L., and Collins, D. R.: The importance of
19 aerosol mixing state and size-resolved composition on CCN concentration and the variation of
20 the importance with atmospheric aging of aerosols, *Atmos. Chem. Phys.*, 10, 7267–7283, 2010.

21 Wang, S., and Flagan, R.: Scanning electrical mobility spectrometer, *J. Aerosol Sci.*, 20, 1485–
22 1488, 1989.

23 Weingartner, E., Burtscher, H., and Baltensperger, U.: Hygroscopic properties of carbon and
24 diesel soot particles, *Atmos. Environ.*, 31, 2311–2327, 10.1016/S1352-2310(97)00023-X, 1997.

25 Wex, H., Hennig, T., Salma, I., Ocskay, R., Kiselev, A., Henning, S., Massling, A.,
26 Wiedensohler, A., and Stratmann, F.: Hygroscopic growth and measured and modeled critical
27 super-saturations of an atmospheric HULIS sample, *Geophys. Res. Lett.*, 34, L02818,
28 10.1029/2006GL028260, 2007.

29 Whitehead, J. D., Irwin, M., Allan, J. D., Good, N., and McFiggans, G.: A meta-analysis of
30 particle water uptake reconciliation studies, *Atmos. Chem. Phys.*, 14, 11833–11841, 2014.

1 Wiedensohler, A., Birmili, W., Nowak, A., Sonntag, A., Weinhold, K., Merkel, M., Wehner,
2 B., Tuch, T., Pfeifer, S., Fiebig, M., Fjåraa, A. M., Asmi, E., Sellegri, K., Depuy, R., Venzac,
3 H., Villani, P., Laj, P., Aalto, P., Ogren, J. A., Swietlicki, E., Williams, P., Roldin, P., Quincey,
4 P., Hüglin, C., Fierz-Schmidhauser, R., Gysel, M., Weingartner, E., Riccobono, F., Santos, S.,
5 Grüning, C., Faloon, K., Beddows, D., Harrison, R., Monahan, C., Jennings, S. G., O'Dowd, C.
6 D., Marinoni, A., Horn, H.-G., Keck, L., Jiang, J., Scheckman, J., McMurry, P. H., Deng, Z.,
7 Zhao, C. S., Moerman, M., Henzing, B., de Leeuw, G., Löschau, G., and Bastian, S.: Mobility
8 particle size spectrometers: harmonization of technical standards and data structure to facilitate
9 high quality long-term observations of atmospheric particle number size distributions, *Atmos.*
10 *Meas. Tech.*, 5, 657–685, 10.5194/amt-5-657-2012, 2012.

11 Wittbom, C., Eriksson, A. C., Rissler, J., Carlsson, J. E., Roldin, P., Nordin, E. Z., Nilsson, P.
12 T., Swietlicki, E., Pagels, J. H., and Svenningsson, B.: Cloud droplet activity changes of soot
13 aerosol upon smog chamber ageing, *Atmos. Chem. Phys.*, 14, 9831–9854, doi:10.5194/acp-14-
14 9831-2014, 2014.

15

16

17

18

19

1 Table 1. Names, location and description of all measurement sites presented in the analysis.

Name of station or <i>campaign</i>	Location	Geographic coordinates	Elevation (m a.m.s.l.)	Site description
Hyytiälä	southern Finland	61°51' N, 24°17' E	181	rural background
Vavihill	southern Sweden	56°01' N, 13°09' E	172	rural background
Jungfraujoch / CLACE-6	Swiss Alps	46°33' N, 07°59' E	3580	free troposphere
Mace Head	west coast of Ireland	53°19' N, 09°54' W	0	coastal background
Pallas	northern Finland	67°58' N, 24°07' E	560	remote background
Finokalia	northern Crete	35°20' N, 25°40' E	250	remote coastal
Cabauw	central Netherlands	51°58' N, 04°56' E	-1	rural background
K-pusza	central Hungary	46°58' N, 19°33' E	125	rural
Chilbolton	southern United Kingdom	51°09' N, 01°26' W	78	continental background
COPS	south-west Germany	48°36' N, 08°12' E	1156	continental background
RHaMBLe	tropical North Atlantic	~21° N, 20° W	0	remote marine
PRIDE-PRD2006	southeastern China	23°33' N, 113°04' E	28	rural background
AMAZE-08	northern Brazil	02°36' S, 60°13' W	108	remote background
CAREBeijing-2006	northern China	39°31' N, 116°18' E	30	suburban

2

3

4

5

1 Table 2. Summary of available data for each measurement location. N_{CCN} is the CCN number concentration, N_{CN} is the total number concentration, A is the
2 activated fraction, D_c is the critical dry diameter and κ is the hygroscopicity parameter. The “setup” column indicates whether the CCNC was operating in
3 polydisperse or monodisperse mode. D_{c_calc} and κ_{calc} have been calculated from polydisperse data using the Differential/Scanning Mobility Particle Sizer
4 (DMPS/SMPS) data.

Name of station or <i>campaign</i>	Setup	Parameters	S_{eff} levels	Time resolution	Reference
Hyttiälä	poly & mono	$N_{CN}, N_{CCN}, A, D_c, \kappa$	0.0859, 0.1, 0.2, 0.216, 0.3, 0.4, 0.478, 0.5, 0.6, 0.74, 1.0, 1.26%	original	Paramonov et al., 2013
Vavihill	poly	$N_{CCN}, N_{CN}, A, D_{c_calc}, \kappa_{calc}$	0.1, 0.2, 0.4, 0.7, 1.0%	original	Fors et al., 2011
Jungfraujoch	poly	$N_{CCN}, N_{CN}, A, D_{c_calc}, \kappa_{calc}$	0.12, 0.24, 0.35, 0.47, 0.59, 0.71, 0.83, 0.95, 1.07, 1.18%	original	Jurányi et al., 2010; Jurányi et al., 2011
Mace Head	poly	N_{CN}, N_{CCN}, A	0.25, 0.5, 0.75%	averaged	Ovadnevaite et al., 2011
Pallas A	poly	$N_{CCN}, N_{CN}, A, D_{c_calc}, \kappa_{calc}$	0.2, 0.4, 0.6, 0.8, 1.0%	original	Jaatinen et al., 2014
Pallas B	poly & mono	$N_{CN}, N_{CCN}, A, D_c, \kappa$	0.47, 0.72, 0.97, 1.22%	averaged (poly), original (mono)	n/a
Pallas C	poly & mono	$N_{CN}, N_{CCN}, A, D_c, \kappa$	0.1, 0.15, 0.2, 0.6, 1.0%	averaged (poly), original (mono)	Brus et al., 2013
Finokalia A	mono	N_{CN}, N_{CCN}, D_c	0.21, 0.38, 0.52, 0.66, 0.73%	averaged	Bougiatioti et al., 2009
Finokalia B	poly	N_{CCN}, A, D_{c_calc}	0.21, 0.38, 0.52, 0.66, 0.73%	averaged	Bougiatioti et al., 2009
Cabauw	poly	N_{CCN}	varies between 0.1 and 1.0%	original	Bègue, 2012

K-pusztá	mono	N_{CCN}, A, κ	0.03, 0.04, 0.10, 0.17, 0.20, 0.25, 0.44, 0.62, 0.67%	averaged	n/a
Chilbolton	mono	N_{CCN}, A, D_c, κ	0.11, 0.30, 0.56, 0.94%	averaged	Whitehead et al., 2014
COPS	poly & mono	N_{CCN}, A, D_c, κ	0.11, 0.17, 0.24, 0.28, 0.32, 0.35, 0.43, 0.50, 0.65, 0.80%	averaged	Irwin et al., 2010; Jones et al., 2011; Whitehead et al., 2014
RHaMBLe	poly & mono	N_{CCN}, A, D_c, κ	0.09, 0.16, 0.29, 0.47, 0.74%	averaged	Good et al., 2010; Whitehead et al., 2014
PRIDE-PRD2006	mono	$N_{CN}, N_{CCN}, A, D_c, \kappa$	0.068, 0.27, 0.47, 0.67, 0.87, 1.27%	original	Rose et al., 2010; Rose et al., 2011
AMAZE-08	mono	$N_{CN}, N_{CCN}, A, D_c, \kappa$	0.095, 0.19, 0.28, 0.46, 0.82%	original	Gunthe et al., 2009
CAREBeijing-2006	mono	$N_{CN}, N_{CCN}, A, D_c, \kappa$	0.066, 0.26, 0.46, 0.66, 0.86%	original	Gunthe et al., 2011
CLACE-6	mono	$N_{CN}, N_{CCN}, A, D_c, \kappa$	0.079, 0.17, 0.27, 0.46, 0.66%	original	Rose et al., 2013

1
2
3
4
5
6
7

- 1 Table 3. Average N_{CCN} concentrations (cm^{-3}) at all studied locations. All N_{CCN} concentrations were recalculated to correspond to the S_{eff} levels suggested
 2 by the ACTRIS Network: 0.1, 0.2, 0.3, 0.5 and 1.0%. The four long-term datasets are shown at the top of the table.

Name of station or campaign	$S_{\text{eff}} = 0.1\%$	$S_{\text{eff}} = 0.2\%$	$S_{\text{eff}} = 0.3\%$	$S_{\text{eff}} = 0.5\%$	$S_{\text{eff}} = 1.0\%$
Vavihill	362	745	952	1285	1795
Hyytiälä	274	407	526	824	1128
Mace Head	472	526	581	691	1007
Jungfraujoch	135	249	341	444	599
<i>PRIDE-PRD2006</i>	1888	4594	6956	9760	13855
<i>CAREBeijing-2006</i>	2547	4751	6510	8460	10711
Cabauw	435	1607	2208	3235	6439
Finokalia B	903	1167	1431	1793	2354
Finokalia A	946	1257	1567	1882	2109
<i>COPS</i>	3	210	364	710	-
<i>RHaMBLe</i>	300	535	717	922	1153
K-pusza	146	349	512	727	834
Chilbolton	145	210	274	384	506
<i>CLACE-6</i>	66	126	156	205	303
Pallas B	-	-	149	176	247
<i>AMAZE-08</i>	37	85	112	136	205
Pallas C	14	38	50	74	141
Pallas A	7	19	31	50	98

1 Table 4. Parameters of the linear fit $A = a \times \ln(S_{\text{eff}}) + b$, for all locations depicted in Fig. 4. a is the slope, b is the intercept and r is the correlation coefficient
 2 of the simple linear regression. The overall linear fit is based on most of the activation curves depicted in Fig. 4, except Finokalia, COPS, Jungfrauoch and
 3 Pallas A, B and C.

Name of station or <i>campaign</i>	a	b	r
Hyytiälä	0.21	0.62	0.99
Vavihill	0.21	0.64	1.00
Jungfrauoch	0.17	0.48	1.00
Mace Head	0.23	0.79	0.98
Finokalia	0.29	0.86	0.99
Pallas A	0.08	0.19	0.99
Pallas B	0.15	0.49	0.98
Pallas C	0.13	0.35	0.98
<i>COPS</i>	0.31	0.92	0.97
<i>RHaMBLe</i>	0.21	0.70	1.00
<i>Pride-PRD2006</i>	0.26	0.74	0.99
<i>AMAZE-08</i>	0.23	0.70	0.99
<i>CARE-Beijing2006</i>	0.22	0.74	1.00
<i>CLACE-6</i>	0.22	0.69	1.00
overall	0.22	0.69	0.96

4

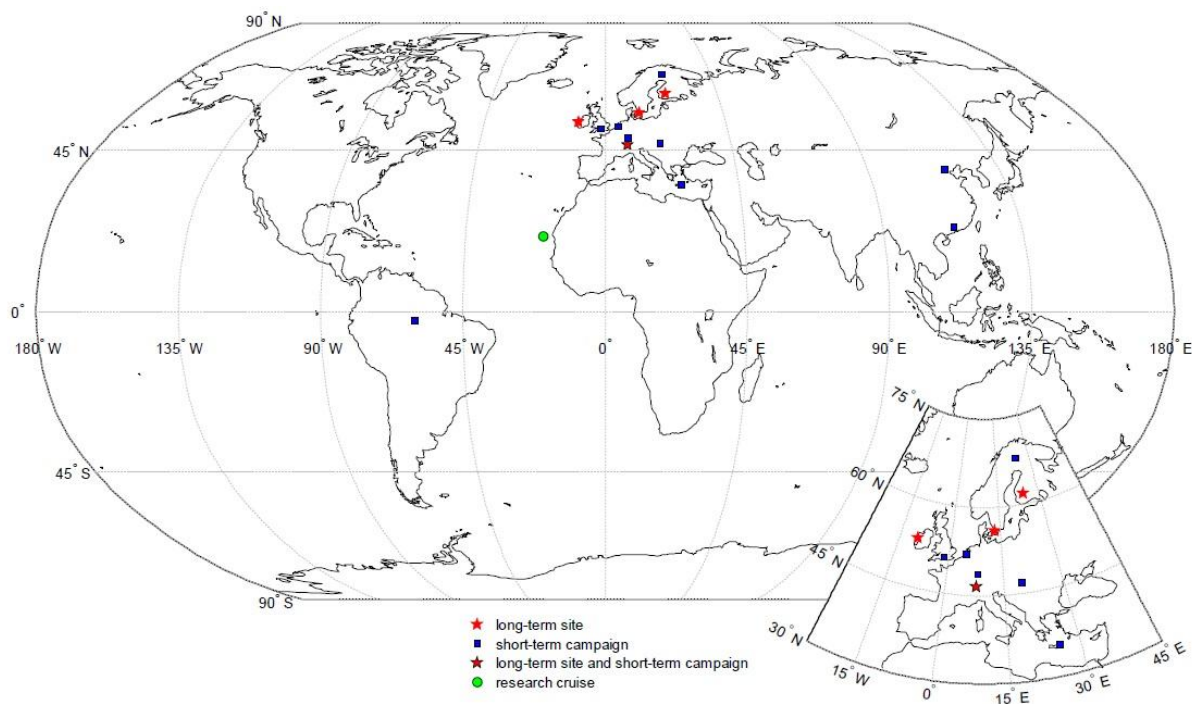
5

6

1 Table 5. Median and percentile κ values for Aitken (< 100 nm) and accumulation (> 100 nm) mode particles for Hyytiälä, Vavihill, Jungfraujoch and Pallas
 2 A and C.

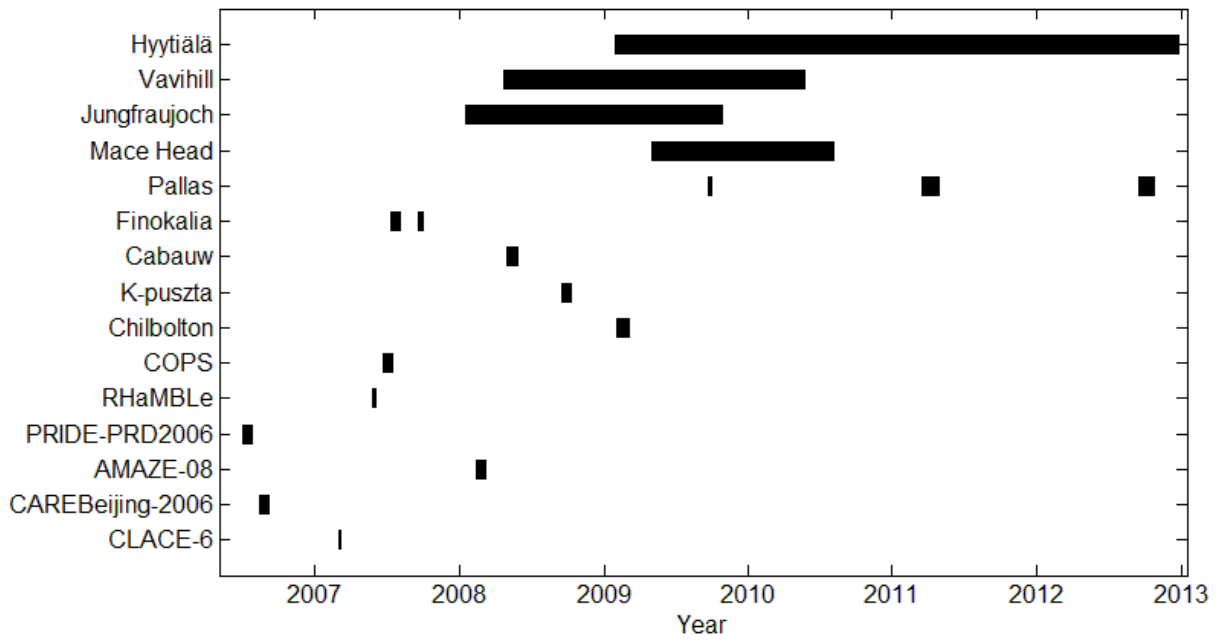
Station	< 100 nm			> 100 nm		
	median	25th percentile	75th percentile	median	25th percentile	75th percentile
Hyytiälä	0.18	0.13	0.27	0.29	0.22	0.45
Vavihill	0.20	0.15	0.28	0.27	0.22	0.33
Jungfraujoch	0.18	0.12	0.28	0.22	0.16	0.31
Pallas A	0.09	0.07	0.13	0.13	0.09	0.20
Pallas C	0.18	0.15	0.27	0.25	0.19	0.37

3
 4
 5
 6
 7
 8
 9
 10
 11
 12



1
 2 Figure 1. A world map showing the locations of CCNC measurements performed during
 3 EUCAARI and presented in this study.

4
 5
 6
 7
 8
 9
 10
 11
 12
 13
 14
 15
 16



1

2 Figure 2. Periods of available data for all locations and campaigns.

3

4

5

6

7

8

9

10

11

12

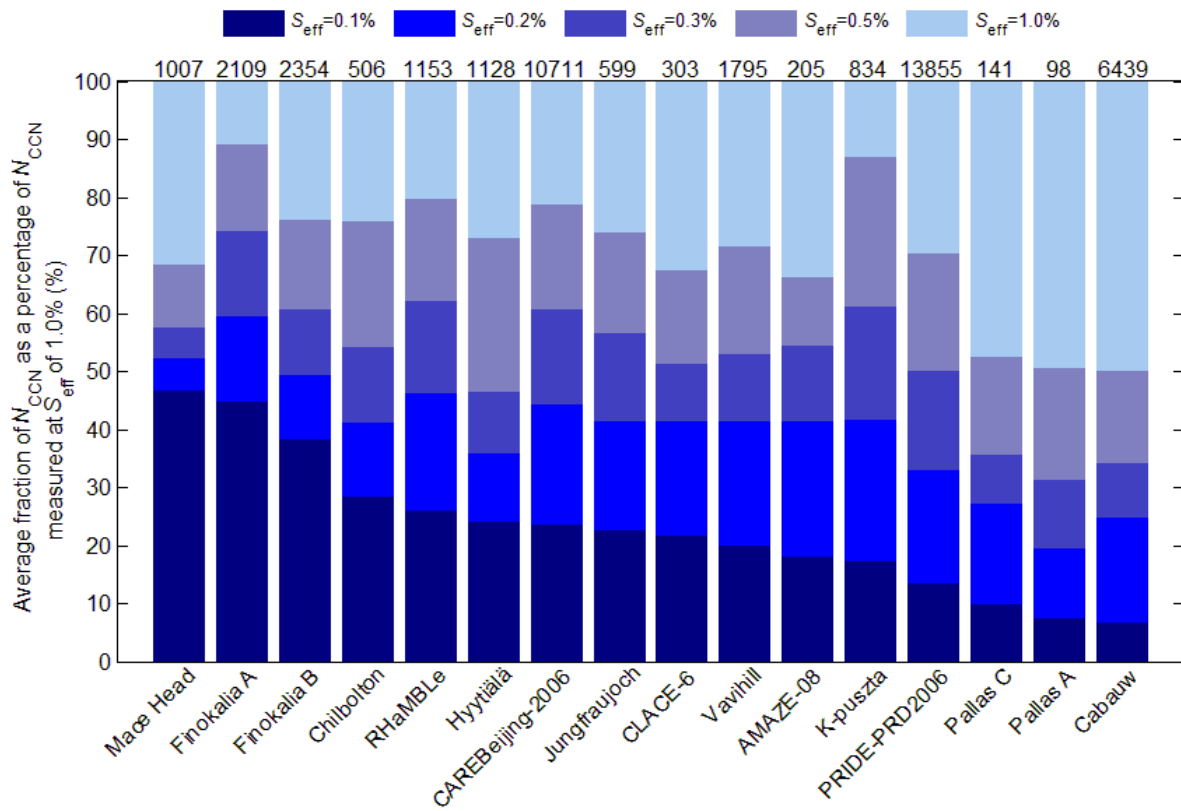
13

14

15

16

17



1

2 Figure 3. Average cumulative N_{CCN} for all available locations shown as a percentage of the
 3 N_{CCN} measured at the S_{eff} of 1.0% (above each bar). Colours indicate the supersaturation S_{eff}
 4 bins.

5

6

7

8

9

10

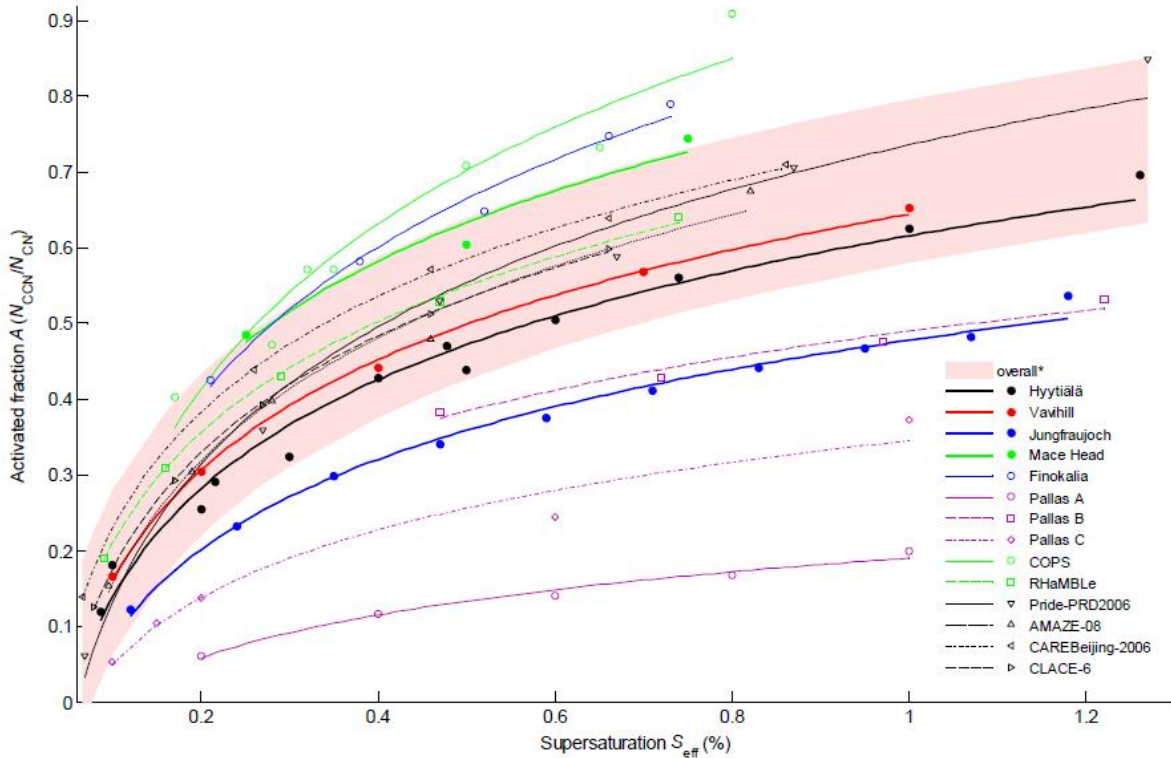
11

12

13

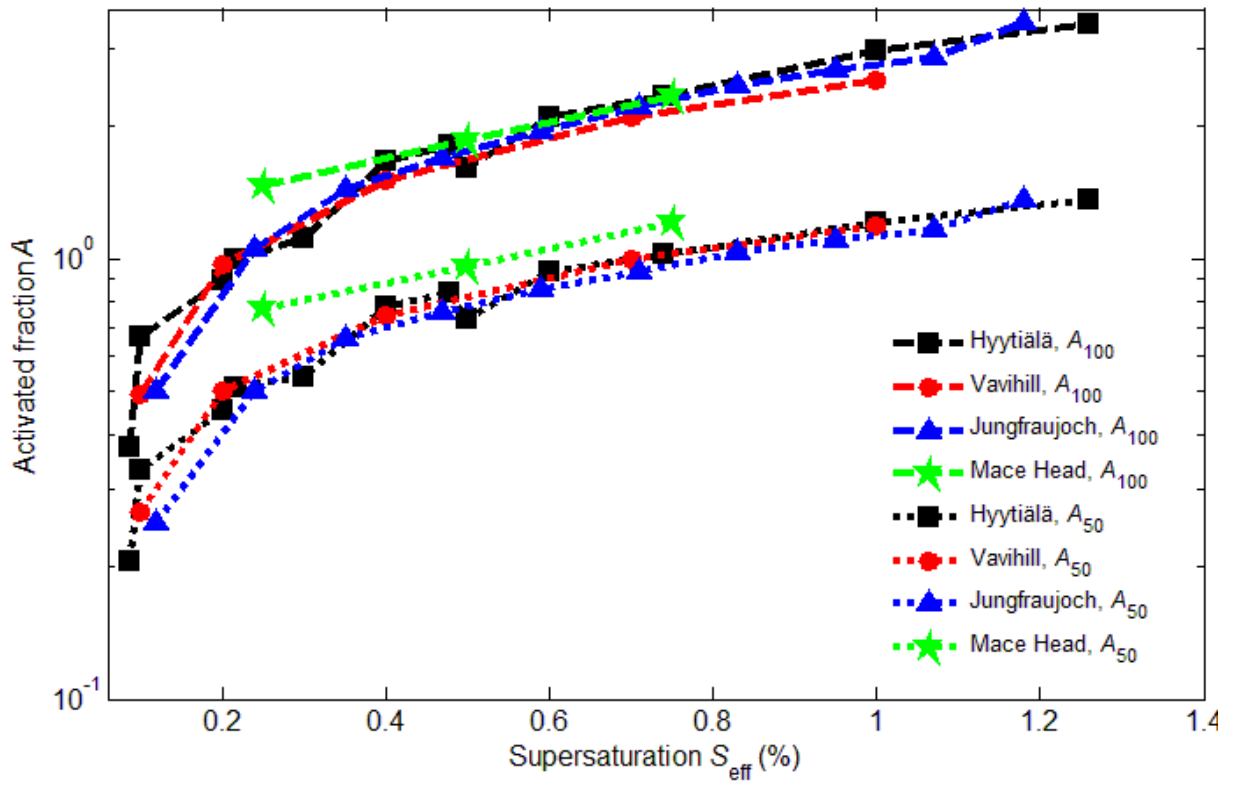
14

15



1
 2 Figure 4. Average activated fraction A as a function of supersaturation S_{eff} for all available
 3 datasets. Symbols represent arithmetic mean values of A calculated from all available data for
 4 each station for each S_{eff} level. Lines represent the linear fits in the form $A = a \times \ln(S_{\text{eff}}) + b$.
 5 Also shown is the overall fit based on most of the data points (*Finokalia, COPS, Jungfraujoch
 6 and Pallas A, B and C datasets excluded). The shading of the overall fit represents the prediction
 7 bounds of the fit with a confidence level of 95%. Slope, intercept and correlation coefficient
 8 values of the linear fits can be found in Table 4.

9
 10
 11
 12
 13
 14
 15
 16



1

2 Figure 5. Average effective activated fractions A_{100} (N_{CCN}/N_{100}) and A_{50} (N_{CCN}/N_{50}) as a function
 3 of supersaturation S_{eff} for the four long-term measurement locations.

4

5

6

7

8

9

10

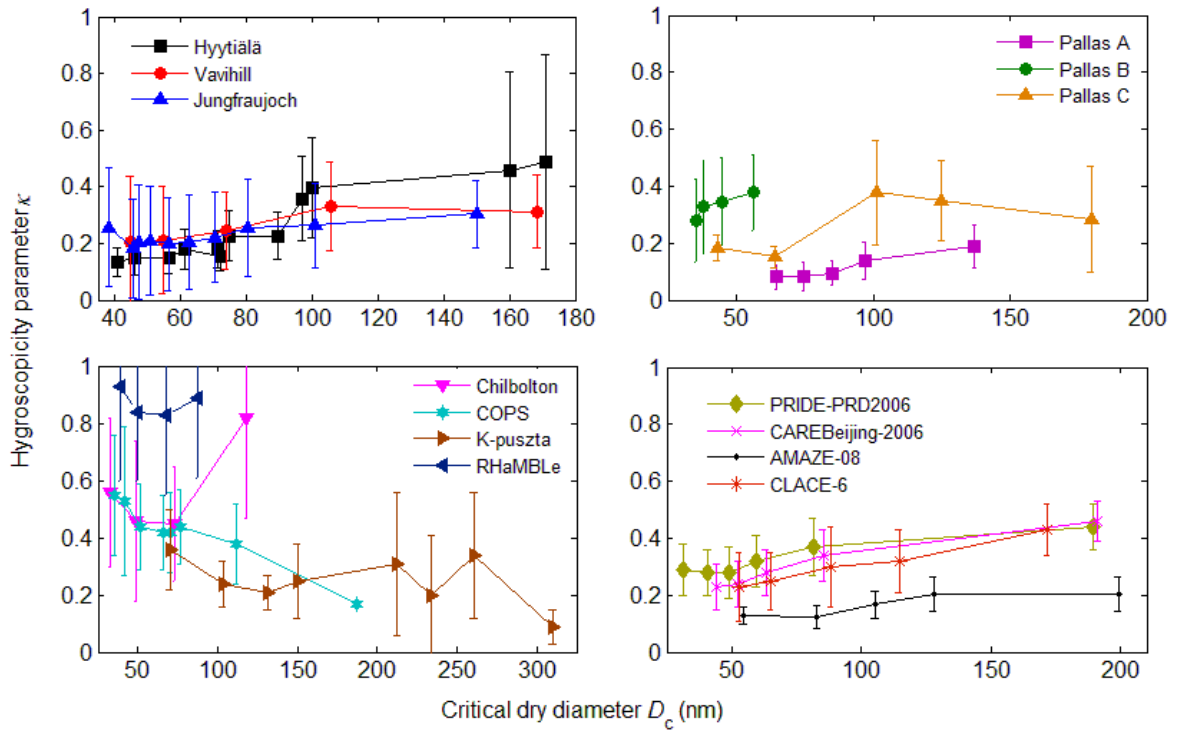
11

12

13

14

15



1

2 Figure 6. Mean hygroscopicity parameter κ as a function of critical dry diameter D_c for selected
 3 locations. Figure split in four panels for more detail. Shown with one standard deviation.

4

5

6

7

8

9

10

11

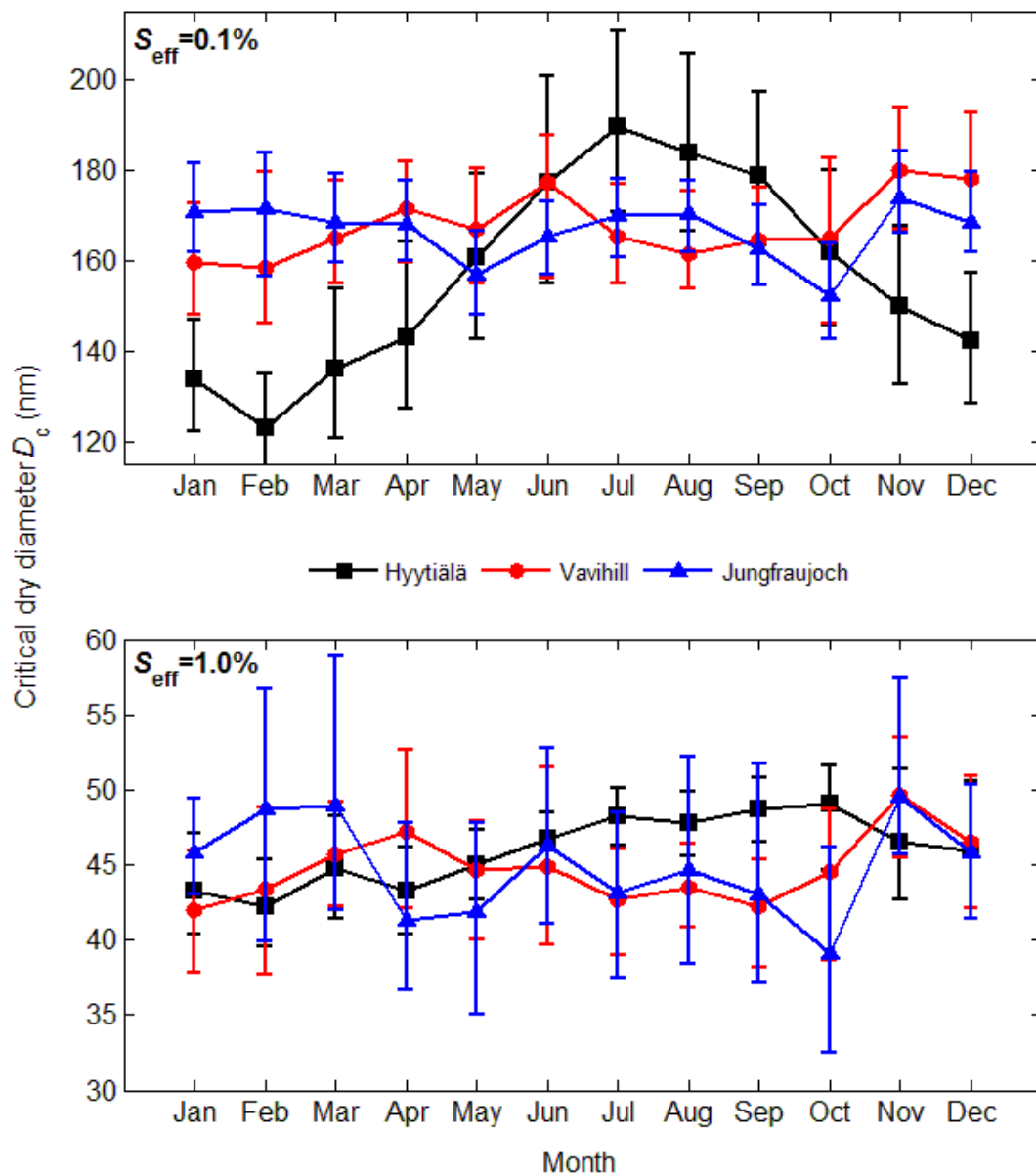
12

13

14

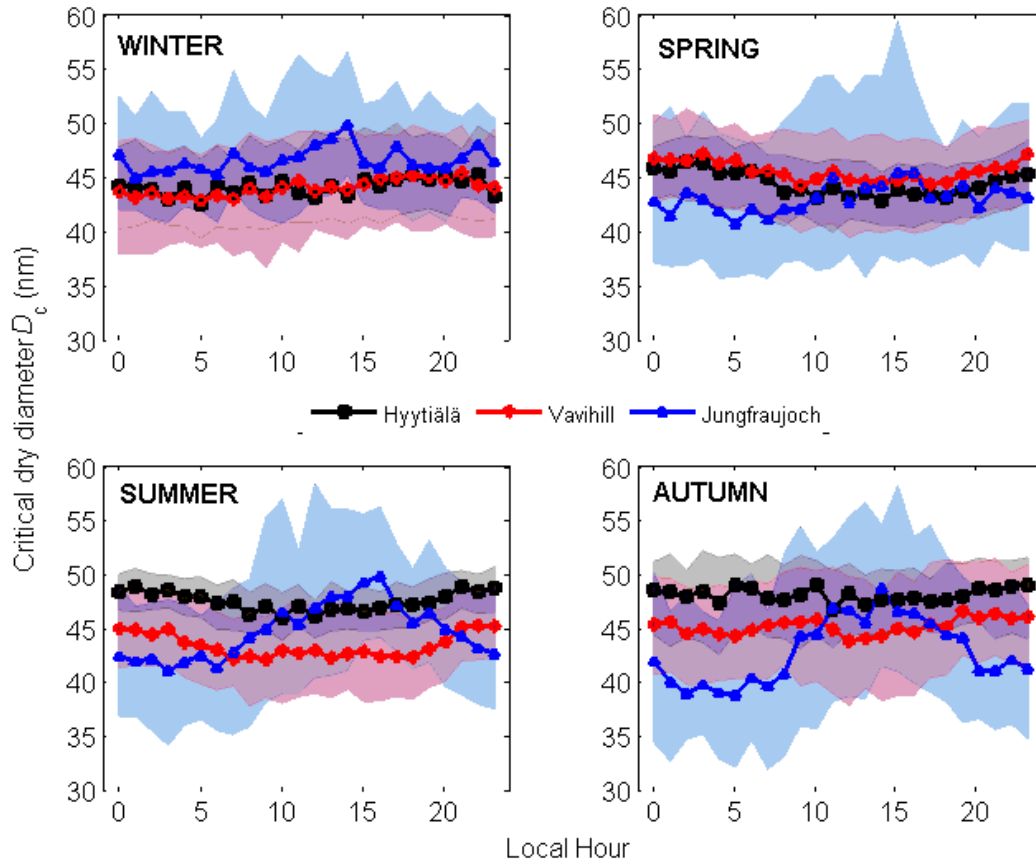
15

16



1
 2 Figure 7. Monthly median D_c at the S_{eff} of 0.1% (upper) and 1.0% (lower) for three long-term
 3 measurement locations. Error bars are 25th and 75th percentiles.

4
 5
 6
 7



1
 2 Figure 8. Hourly median critical dry diameters D_c at the S_{eff} of 1.0% for three long-term
 3 measurement locations separated by seasons. Shaded areas represent the 25th and 75th
 4 percentiles, with colours corresponding to the median data series.